Hierarchical Structure of Magnetohydrodynamic Turbulence in Position-Position-Velocity Space

Draft version June 22, 2012
Preprint typeset using LaTeX style emulateapj v. 5/2/11

HIERARCHICAL STRUCTURE OF MAGNETOHYDRODYNAMIC TURBULENCE IN POSITION-POSITION-VELOCITY SPACE

Blakesley Burkhart[1], A. Lazarian[1], Alyssa Goodman[2], Erik Rosolowsky[3]

Draft version June 22, 2012

ABSTRACT

Magnetohydrodynamic turbulence is able to create hierarchical structures in the interstellar medium that are correlated on a wide range of scales via the energy cascade. We use hierarchical tree diagrams known as dendrograms to characterize structures in synthetic Position-Position-Velocity (PPV) emission cubes of optically thin isothermal magnetohydrodynamic turbulence. We show that the structures and degree of hierarchy observed in PPV space are related to the physics of the gas, i.e. self-gravity and the global sonic and Alfvénic Mach number. Simulations with higher Alfvénic Mach number, self-gravity and supersonic flows display enhanced hierarchical structure. We observed a strong sonic and Alfvénic dependency when we apply the the statistical moments (i.e. mean, variance, skewness, kurtosis) to the dendrogram distribution. Larger magnetic field and sonic Mach number correspond to larger values of the moments. Application of the dendrogram to 3D density cubes, also known as Position-Position-Position cubes (PPP), reveals that the dominant emission contours in PPP and PPV are related for supersonic gas but not for subsonic. We also explore the effects of smoothing, thermal broadening and velocity resolution on the dendrograms in order to make our study more applicable to observational data. These results all point to hierarchical tree diagrams as being a promising additional tool for studying ISM turbulence and star forming regions in the direction of obtaining information on the degree of self-gravity, the Mach numbers and the complicated relationship between PPV and PPP.

Subject headings: ISM: structure — MHD — turbulence

1. INTRODUCTION

The current understanding of the interstellar medium (ISM) is that it is a multi-phase environment composed of a tenuous plasma, consisting of gas and dust, which is both magnetized and highly turbulent (Ferriere 2001; McKee & Ostriker 2007). In particular, magnetohydrodynamic (MHD) turbulence is essential to many astrophysical phenomena such as star formation, cosmic ray dispersion, and many transport processes. (see Elmegreen & Scalo 2004; Ballesteros-Paredes et al. 2007 and references therein). Additionally, turbulence has the unique ability to transfer energy over scales ranging from kiloparsecs down to the proton gyroradius. This is critical for the ISM, as it explains how energy is distributed from large to small spatial scales in the Galaxy.

Observationally, several techniques exist to study MHD turbulence in different ISM phases. Many of these techniques focus on the density fluctuations in ionized media (Armstrong et al. 1995; Chepurnov & Lazarian 2010), fluctuations in spectroscopic data and column density maps for neutral media (Spangler & Gwinn 1990; Padoan et al. 2003) , or gradients of linear polarization maps (Haverkorn & Heitsch 2004; Gaensler et al. 2011; Burkhart, Lazarian & Gaensler 2012). For studies of turbulence, spectroscopic data has a clear advantage in that it contains information about the turbulent velocity field as well as the density fluctuations. However, density and velocity are entangled in PPV space, making the interpretation of this type of data difficult. For the separation of the density and velocity fluctuations, special techniques such as the Velocity Coordinate Spectrum (VCS) and the Velocity Channel Analysis (VCA) have been developed (Lazarian & Pogosyan 2000, 2004, 2006, 2008).

Most of the efforts to relate observations and simulations of magnetized turbulence are based on obtaining the spectral index (i.e. the log-log slope of the power spectrum) of either the density and/or velocity (Lazarian & Esquivel 2003; Esquivel & Lazarian 2005; Ossenkopf et al. 2006). However, the power spectrum alone does not provide a full description of turbulence, as it only contains the Fourier amplitudes and neglects information on phases. This fact combined with the knowledge that astrophysical turbulence is complex, with multiple injection scales occurring in a multiphase medium, points to researchers needing additional ways of analyzing observational and numerical data in the context of turbulence. In particular these technique studies are currently focused into two categories:

- Development: Test and develop techniques that will complement and build off of the theoretical and practical picture of a turbulent ISM that the power spectrum presents.
- Synergy: Use several techniques simultaneously to obtain an accurate picture of the parameters of turbulence in the observations.

In regards to the first point, there has been substantial progress in the development of techniques to study turbulence in the last decade. Techniques for the study

[1] Astronomy Department, University of Wisconsin, Madison, 475 N. Charter St., WI 53711, USA
[2] Harvard-Smithsonian Center for Astrophysics, 60 Garden Street, MS-78, Cambridge, MA 02138
[3] University of British Columbia, Okanagan Campus,3333 University Way, Kelowna BC V1V 1V7, Canada

of turbulence can be tested empirically using parameter studies of numerical simulations or with the aid of analytical predictions (as was done in the case of VCA). In the former, the parameters to be varied (see Burkhart & Lazarian 2011) include the Reynolds number, sonic and Alfvénic Mach number, injection scale, equation of state, and, for studies of molecular clouds, should include radiative transfer and self-gravity (see Ossenkopf 2002; Padoan et al. 2003; Goodman et al. 2009). Some recently developed techniques include the application of probability distribution functions (PDFs), wavelets, spectral correlation function (SCF),[4] delta-variance, the principal component analysis, higher order moments, Genus, Tsallis statistics, spectrum and bispectrum (Gill & Henriksen 1990; Stutzki et al. 1998; Rosolowsky et al. 1999; Brunt & Heyer 2002; Kowal, Lazarian & Beresnyak 2007; Chepurnov et al. 2008; Burkhart et al. 2009; Esquivel & Lazarian 2010; Tofflemire et al. 2011). Additionally, these techniques are being tested and applied to different wavelengths and types of data. For example, the PDFs and their mathematical descriptors have been applied to the *observations* in the context of turbulence in numerous works using different data sets including: linear polarization data (see Gaensler et al. 2011; Burkhart, Lazarian, & Gaensler 2012), HI column density of the SMC (Burkhart et al. 2010), molecular/ dust extinction maps (Goodman, Pineda, & Schnee 2009; Brunt 2010; Kainulainen et al. 2011) and emission measure and volume averaged density in diffuse ionized gas (Hill et al. 2008; Berkhuijsen & Fletcher 2008).

The latter point in regard to the synergetic use of tools for ISM turbulence is only recently being attempted as many techniques are still in the stages of being developed. However, this approach was used in Burkhart et al. 2010, which applied spectrum, bispectrum and higher order moments to H I column density of the SMC. The consistency of results obtained with a variety of statistics and compared with more traditional observational methods made this study of turbulence in the SMC a promising first step.

This paper falls under the category of "technique development." In particular, we investigate the utility of dendrograms in studying the hierarchical structure of ISM clouds. It has long been known that turbulence is able to create hierarchical structures in the ISM (Scalo 1985, 1990; Vazquez-Semadeni 1993 ;Stutzki 1998), however many questions remain, such as what type of turbulence is behind the creation of this hierarchy and what is the role of self-gravity and magnetic fields? Hierarchical structure in relation to these questions is particularly important for the star formation problem (Larson 1981; Elmegreen & Elmegreen 1983; Feitzinger & Galinski 1987; Elmegreen 2011).

The earliest attempts to characterize ISM hierarchy utilized tree diagrams as a mechanism for reducing the data down to hierarchical 'skeleton images' (see Houlahan & Scalo 1992). More recently dendrograms have been used on ISM data in order to characterize self-gravitating structures in star forming molecular clouds (Rosolowsky et al. 2008 and Goodman et al. 2009). A dendrogram (from the Greek dendron "tree",- gramma "drawing") is a hierarchical tree diagram that has been used extensively in other fields, particularly in computational biology, and occasionally in galaxy evolution (see Sawlaw & Haque-Copilah 1998 and Podani, Engloner, & Major 2009 for examples). Rosolowsky et al. (2008) and Goodman et al. (2009) used the dendrogram on spectral line data of L1448 to estimate key physical properties associated with isosurfaces of local emission maxima such as radius, velocity dispersion, and luminosity. These works provided a new and promising way of characterizing self-gravitating structures and properties of molecular clouds through the application of dendrogram to ^{13}CO(J=1-0) PPV data.

In this paper we apply the dendrogram to synthetic observations (specifically PPV cubes) of isothermal MHD turbulence in order to investigate the physical mechanisms behind the gas hierarchy. Additionally, we are interested in the nature of the structures that are found in PPV data and how these structures are related to both the physics of the gas and the underlying density and velocity fluctuations generated by turbulence. Simulations provide an excellent testing ground for this problem, as one can identify which features in PPV space are density features and which are caused by velocity crowding. Furthermore, one can answer the question of under what conditions do the features in PPV relate back to the 3D density or PPP cube?

In order to answer these questions we perform a parameter study using the dendrogram. We focus on how changing the global parameters of the turbulence, such as the sonic Mach number, Alfvénic Mach number and level of self-gravity affect the amount of hierarchy observed, the relationship between the density and velocity structures in PPV, and the number and statistical distribution of dominate emission structures. Along with the Reynolds number, the sonic and Alfvénic Mach numbers are useful descriptors of the turbulence and are critical to several phenomena in astrophysics, including cosmic ray acceleration, turbulent magnetic reconnection, ambipolar diffusion and structure formation in the ISM. They are defined as the ratio of the flow velocity to the sound speed and Alfvén speed, respectively. That is, the sonic Mach number is $\mathcal{M}_s \equiv V_L/c_s$, where V_L is the injection velocity, c_s is the sound velocity, and the Alfvénic Mach number is $\mathcal{M}_A \equiv V_L/V_A$, where V_A is the Alfvén velocity. The Sonic Mach number provides important clues on the role of fluid compressibility while the Alfvénic Mach number gives insight into the influence of the magnetic field in the evolution of ISM turbulence. Throughout the paper we will use the terms "compressibility" and Sonic Mach number interchangeably.

The paper is organized as follows. In § 2 we describe the dendrogram algorithm, in § 3 we discuss the simulations and provide a description of the MHD models. We investigate the physical mechanisms that create hierarchical structure in the dendrogram tree and as well as characterize the tree diagrams via statistical moments in § 4. In § 5 we compare the dendrograms of PPP and PPV. In § 6 we discuss application and investigate issues of resolution. Finally, in § 7 we discuss our results followed by the conclusions in § 8.

[4] The similarities between VCA and SCF are discussed in Lazarian (2009).

2. DENDROGRAM ALGORITHM

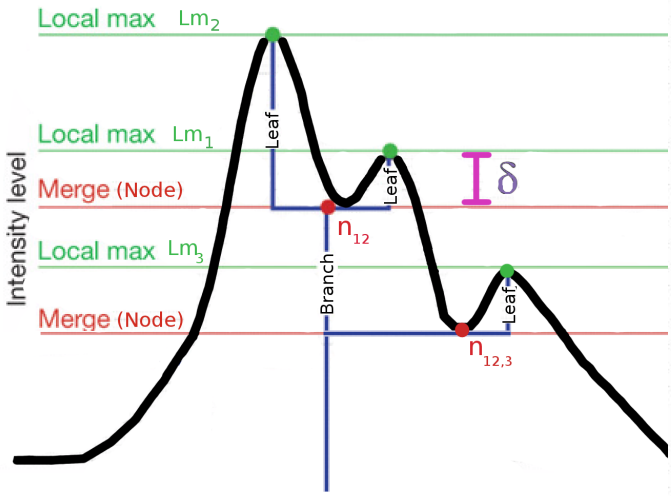

FIG. 1.— The dendrogram for a hypothetical 1D emission profile showing three local maximum (leaves) and merger points (nodes). The Dendrogram is shown in blue and can be altered by changing the threshold level δ to higher or lower values. In this example, increasing the value of δ will merge the smallest leaf into the larger structure. The local maximum (green dots) and merger points (i.e. nodes, red dot) are the values used to create a distribution ξ.

Run	$M_s\approx$	$M_A\approx$	Sonic Nature	Magnetic Nature	Size	Comments
1	0.5	0.7	sub-sonic	sub-Alfvénic	512x512x512	
2	0.7	0.7				
3	2	0.7	super-sonic			
4	3	0.7				
5	4.4	0.7				
6	7	0.7				
7	8.4	0.7				
8	10	0.7				
9	0.5	2	sub-sonic	super-Alfvénic		
10	0.7	2				
11	2	2	super-sonic			
12	3	2				
13	4.4	2				
14	7	2				
15	8.4	2				
16	10	2				
17	2	2				
18	2	0.7		sub-Alfvénic	256x256x256	
19	2	2		super-Alfvénic		self-gravityx4
20	2	2				self-gravityx1

FIG. 2.— List of the simulations and their properties. We use different colors to differentiate the parameter space. We define the subsonic regimes as anything less then $\mathcal{M}_s$=1 and the supersonic regime as $\mathcal{M}_s > 1$. Two Alfvénic regimes exist for each sonic Mach number: super-Alfvénic and sub-Alfvénic.

The dendrogram is a tree diagram that can be used in 1D, 2D or 3D spaces to characterize how and where local maxima merge as a function of a threshold parameter. Although this paper uses the dendrogram in 3D PPV space to characterize the merger of local maxima of emission, it is more intuitive to understand the 1D and 2D applications. A 1D example of the dendrogram algorithm for an emission profile is shown in Figure 1. In this case, the threshold value is called δ, and is the minimum amplitude above a merger point that a local maximum must be before it is considered distinct. That is, if a merger point (or node) is given by n and a local maximum is given by Lm then in order for a given local max Lm_1 to be considered significant, $Lm_1 - n_{1,2} > \delta$. If $Lm_1 - n_{1,2} \leq \delta$. then Lm_1 would merge into Lm_2 and no longer be considered distinct.

For 2D data, a common analogy (see Houlahan & Scalo 1992, Rosolowsky et al. 2008) is to think of the dendrogram technique as a descriptor of an underwater mountain chain. As the water level is lowered, first one would see the peaks of the mountain, then mountain valleys (saddle points) and as more water is drained, the peaks may merge together into larger objects. The dendrogram stores information about the peaks and merger levels of the mountain chain.

The dendrogram is similar to many other statistics that employ a user defined threshold value in order to classify structure. By varying the threshold parameter δ (see Figure 1), different dendrogram local max distributions are created. An example of another statistic that utilizes a density/emission threshold value is the Genus statistic, which has proven useful for studying ISM topology (Lazarian, Pogosyan & Esquivel 2002; Lazarian 2004; Kim & Park 2007; Kowal et al. 2007; Chepurnov et al. 2008). For the Genus technique, the variation of the threshold value is a critical point in understanding the topology of the data in question.

For our purposes, we examine the dendrogram in 3D PPV space (see Rosolowsky et al. 2008; Goodman et al. 2009 for more information on the dendrogram algorithm applied in PPV). In the 3D case, it is useful to think of each point in the dendrogram as representing a 3D contour (isosurface) in the data cube at a given level. As δ sets the definition for "local maximum," setting it too high will produce a dendrogram that may miss important substructures while setting it very low may produce a dendrogram that is dominated by noise. While δ sets the value for the minimum leaf length, the branches of the tree do not directly depend on δ, and only depend on at what intensity level a set of local maximum are joined at.

The issues of noise and the dendrogram were discussed extensively in Rosolowsky et al. 2008. While the dendrogram is designed to present only the essential features of the data, noise will mask the low-amplitude or high spatial frequency variation in the emission structures. In extreme cases where the threshold value is not set high enough or the signal-to-noise is very low, noise can result in local maxima that do not correspond to real structure. As a result, the algorithm has a built in noise suppression criteria which only recognizes structures that have 4 σ_{rms} significance above δ. Such a criterion has been previously used in data cube analysis as noise fluctuations will typically produce 1 σ_{rms} variations (Brunt et al. 2003; Rosolowsky & Blitz 2005; Rosolowsky et al. 2008).

Once the dendrogram is created, there are multiple ways of viewing the information it provides such as:

- A tree diagram (the dendrogram itself).
- 3D viewing of the isocontours and their connectivity in PPV space.
- A histogram of the dendrogram leaf and node values (i.e. intensities), which can then be further

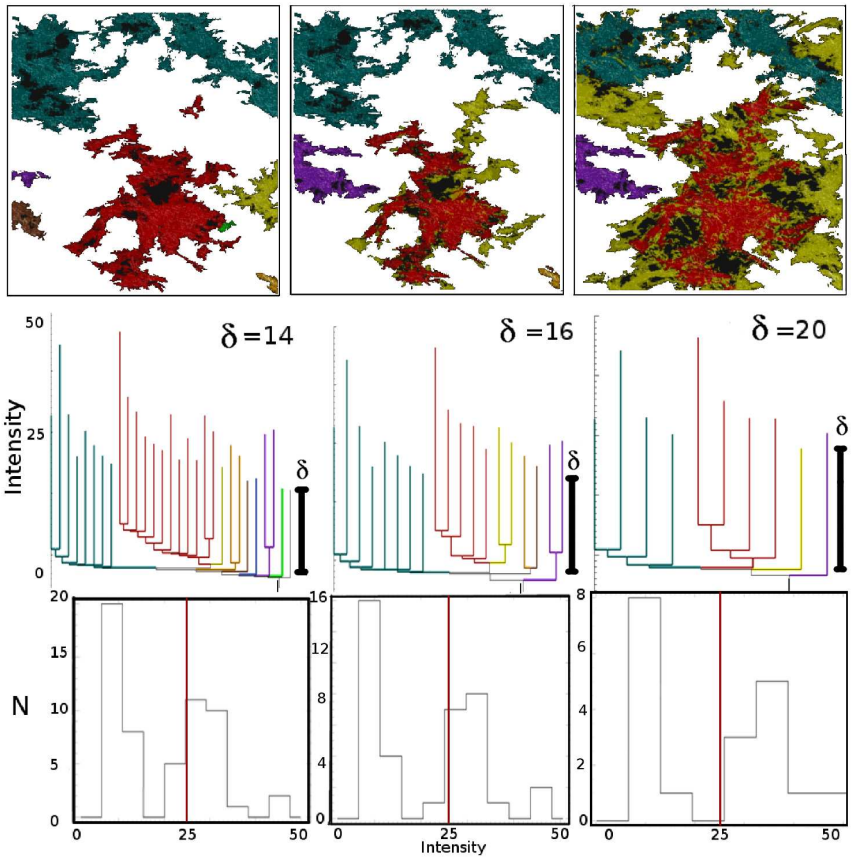

FIG. 3.— Different ways of viewing dendrogram information used in this paper. Here we show an example for supersonic sub-Alfvénic turbulence (model 3 from Figure 2) for threshold values δ=14,16,20 (left, center, right columns). The top row represents the isosurfaces in the PPV data and the middle row is the corresponding dendrogram (the black line is a reference marker for δ) with colors matching to the isosurface structures. Note there is no information on the x-axis of the tree diagram as the branches are sorted not to cross. However this still preserves all information about connectivity and hierarchy at the expense of positional information. The bottom row is the histogram of the resulting tree diagram, including the leaves, branches and nodes. The red line is a reference marker at intensity level 25. The units of intensity on the y-axis of the tree diagrams in the middle row could be in brightness temperature (T_b) for scaled simulations or observations.

statistically analyzed.

We note that this third point is a novel interpretation of the dendrogram that we develop in this work. Here the histogram will be composed of intensity values important to the hierarchical structure of the image. This includes the leaves, denoted by Lm, and nodes, denoted with n. In this case we define a distribution:

$$\xi = \begin{pmatrix} Lm_1 & Lm_2 & Lm_3 & Lm_4 .... Lm_n \\ n_{1,2} & n_{3,4} & n_{(1,2),(3,4)} & ...n_{m,n} \end{pmatrix}$$

This interpretation is visualized in Figure 3 and further described below. To produce the dendrogram, we first identify a population of local maxima as the points which are larger than all surrounding voxels touching along the face (not along edges or corners). This large set of local maxima is then reduced by examining each maximum and searching for the smallest contour level that contains only that maximum. If this contour level is less than δ below the local maximum, that local maximum is removed from consideration in the leaf population (this difference in data values is the vertical length of the "leaves" of the dendrogram).

Once the leaves (local maxima) of the dendrogram are established, we contour the data with a large number of levels (500 specifically, see Rosolowsky et al. 2008; Goodman et al. 2009). The dendrogram "branches" are graphically constructed by connecting the various sets of maxima at the contour levels where they are joined (see Figure 1 for a 1D example). For graphical presentation, the leaves of the structure tree are shuffled until the branches do not cross when plotting. As a result, the x-axis of the dendrogram contains no information. More information on the dendrogram algorithm can be found in Goodman et al. (2009) in the Supplementary Methods section and in Rosolowsky et al. (2008).

The purpose of this paper is to use dendrogram to characterize the observed hierarchy seen in the data. We are not necessarily interested in individual clumps found in the synthetic PPV data, but rather characterizing how the structures and hierarchy found in simulations of MHD turbulence depend on parameters such as the level of turbulence, magnetic fields, and self-gravity. While turbulence has often been cited as the cause of the observed hierarchical structure in the ISM (Stutzki 1998), it is unclear to what extent magnetic fields, gas pressure, and gravity play roles in the creation of ISM hierarchy even though these parameters are known to drastically change the PDF and spectrum of both column density and PPV data (see Falgarone 1994; Kowal et al. 2007; Tofflemire et al. 2011).

3. DATA

We generate a database of twenty 3D numerical simulations of isothermal compressible (MHD) turbulence by

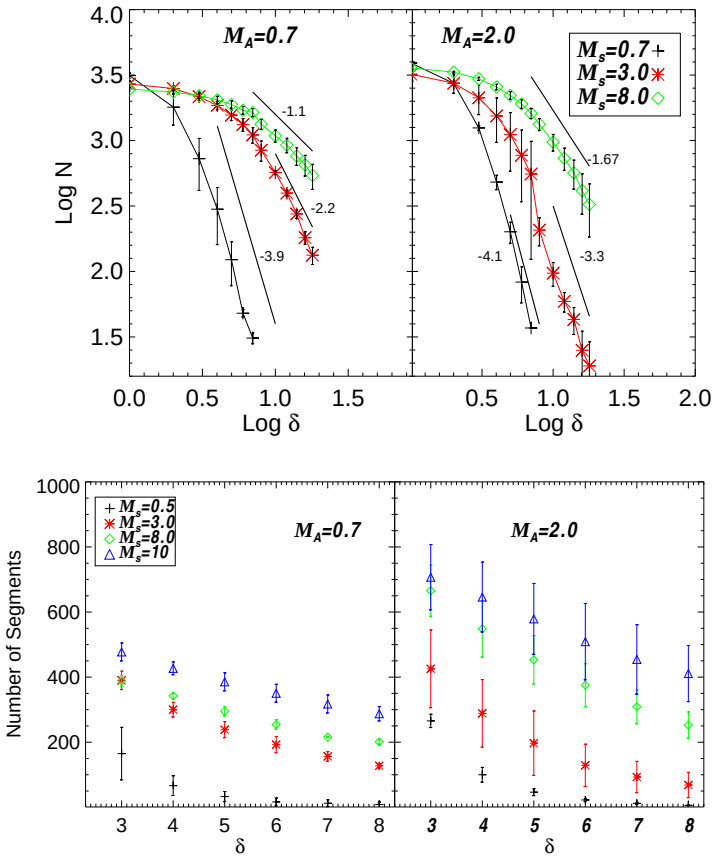

FIG. 4.— Top: Number of Structures (leaves and branches) vs. δ for six different simulations. Error bars are created by running the analysis for multiple time snapshots of the well-developed turbulence. Bottom: Number of segments from root to leaf on the largest branch of the tree vs. δ. The left panel is shows higher magnetization (sub-Alfvénic) while the right shows lower magnetization (super-Alfvénic). Both panels have the y-axis set to the same range for ease of comparison. Hierarchical structure is created both by shocks (high sonic Mach number cases) and a high Alfvénic Mach number).

using the MHD code of Cho & Lazarian 2003 and vary the input values for the sonic and Alfvénic Mach number. We briefly outline the major points of the numerical setup.

The code is a second-order-accurate hybrid essentially non-oscillatory (ENO) scheme which solves the ideal MHD equations in a periodic box:

$$\frac{\partial \rho}{\partial t} + \nabla \cdot (\rho \mathbf{v}) = 0, \quad (1)$$

$$\frac{\partial \rho \mathbf{v}}{\partial t} + \nabla \cdot \left[\rho \mathbf{v}\mathbf{v} + \left(p + \frac{B^2}{8\pi} \right) \mathbf{I} - \frac{1}{4\pi} \mathbf{B}\mathbf{B} \right] = \mathbf{f}, \quad (2)$$

$$\frac{\partial \mathbf{B}}{\partial t} - \nabla \times (\mathbf{v} \times \mathbf{B}) = 0, \quad (3)$$

with zero-divergence condition $\nabla \cdot \mathbf{B} = 0$, and an isothermal equation of state $p = C_s^2 \rho$, where p is the gas pressure. On the right-hand side, the source term $\mathbf{f}$ is a random large-scale driving force. We drive turbulence solenoidally[5] with energy injected on the large scales. The time t is in units of the large eddy turnover time ($\sim L/\delta V$) and the length in units of L, the scale of energy injection. The magnetic field consists of the uniform background field and a fluctuating field: $\mathbf{B} = \mathbf{B}_{\rm ext} + \mathbf{b}$. Initially $\mathbf{b} = 0$. We stress that simulations are scale free and all units are related to the turnover time and energy injection scale.

We divide our models into two groups corresponding to sub-Alfvénic and super-Alfvénic turbulence. For each group we computed several models with different values of gas pressure (see Figure 2) falling into regimes of subsonic and supersonic. We ran 14 compressible MHD turbulent models, with 512^3 resolution, and 4 at 256^3 with 2 of these having self-gravity. We solve for the gravitation potential using a Fourier method similar to that described in Ostriker et al. 1999. The models are listed and described in Figure 2.

We use density and velocity perpendicular to the mean magnetic field in order to create fully optically thin synthetic PPV data cubes, although we also investigate dendrogram for other LOS orientations. The PPP and synthetic PPV cubes are all normalized by the mean value, i.e. $PPV_{final} = PPV_{orignial} / < PPV_{orignial} >$) Varying the optical depth will be done in a later work. We create cubes with a given velocity resolution of 0.07, which is ten times smaller then the rms velocity of the simulation ($v_{rms} = 0.7$). For reference, the sound speed of the simulations varies from $c_s = 1.4 - 0.07$ for our most subsonic to most supersonic simulations. PPV cubes are created by reorganizing density cubes into channel bins based on given velocity intervals. Additional discussion on comparing the simulations to observations is found in Section 6.

[5] The differences between solenoidal and compressive driving is discussed more in Federrath et al. 2008. One can expect driving in the ISM to be a combination of solenoidal and compressive, however both types of driving will produce shocks on a range of scales, which is what we study here.

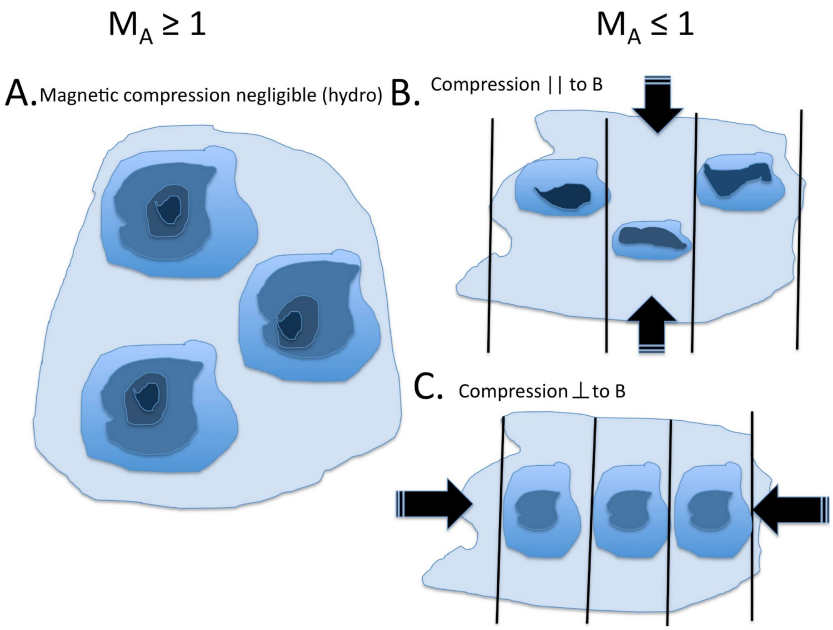

FIG. 5.— Illustration of supersonic clouds with different magnetic regimes and how this affects the observed clumps. Panel A shows a case with very low Alfvénic Mach number or a case of hydrodynamic turbulence. In this case, turbulence allows the creation of hierarchical structure with no limitation on the gas motion. Panels B and C show a cloud with higher magnetization (sub-Alfvénic) with compression parallel and perpendicular to the field lines. In the sub-Alfvenic cloud, motions will be correlated due to the strong field and the magnetic field will restrict shock compression perpendicular to the field lines (panel C). For shocks parallel to the field (panel B), increased compression will occur which will enhance contour contrast and decrease hierarchy.

4. CHARACTERIZING HIERARCHY AND STRUCTURES CREATED BY TURBULENCE

We applied the dendrogram algorithm on synthetic PPV cubes with various sonic and Alfvénic Mach numbers. An example of how the the tree diagram output changes with threshold value δ is shown in Figure 3. The top row of Figure 3 shows the isosurfaces with the colors relating back to the colors in the corresponding dendrogram shown in the middle row. As the threshold intensity value δ (which, shown here with a black line, sets the definition of the local maximum or 'leaves of the tree') increases, structures in the dendrogram begin to merge with each other. The leaf and branch length and number of structures provides information on the hierarchical nature of the PPV cube. The branches are sorted to not cross, which leaves the x-axis with no information. The bottom row of Figure 3 shows the histograms of the dendrogram distribution of intensities (leaves and nodes). The red line is a reference line at intensity level 25. This distribution also changes with changing threshold value, as leaves merge with one another and the hierarchy changes.

In the next subsections, we investigate the effects of the compressibility, magnetization, and level of self-gravity on the number of structures, amount of hierarchical structure, and moments of the dendrogram distribution. We define a hierarchical dendrogram as one which has many segments on its paths and hence many levels above the root.

4.1. *Sonic and Alfvenic Mach Numbers*

4.1.1. *Leaf and Branch Counting*

We computed the dendrogram for all synthetic non-self gravitating PPV cubes with varying threshold values.

Figure 4 top shows how the total number of structures (i.e., dominant emission contours including dendrogram "leaves and branches") changes as we change δ. We plot the total number of structures vs. δ on a logarithmic scale (i.e. Log N vs Log δ) for simulations with three differing values of sonic Mach number ($\mathcal{M}_s$=8.0, 3.0, 0.7) and two values of Alfvénic Mach number. The left panel shows sub-Alfvénic models and the right shows super-Alfvénic models. Error bars are created by taking the standard deviation between different time snapshots. We note that power law tails can be seen at values of δ past the mean value (i.e. past log $\delta = 0$). We over plot the values of the slopes with solid black lines for reference.

When δ is at or slightly below the mean value of the data cubes, there is little difference in number of structures seen in the dendrogram between simulations of different sonic Mach number. This is surprising, since the structures seen in subsonic turbulence are very different from supersonic case. In the regime where δ is at the mean value, we are sampling most of the PPV cube emission and therefore are not sensitive to the differences seen at larger threshold values which will merge low intensity structures. Once we increase δ beyond the mean however, the number of structures between the subsonic (black plus signs) and supersonic simulations (red stars and green diamonds) rapidly diverges as the emission contours due to shocks begin to stand out, and the low intensity contours merge. Because shocks create higher intensity values in the PPV cubes, the slopes in the subsonic cases are much steeper as the number of structures the dendrogram considers significant at a given threshold value rapidly falls off to zero. Subsonic models have fewer significant emission contours since they do not have density enhancements created by shocks and therefore the density/velocity contrast between subsonic and supersonic turbulence becomes clear at higher threshold values. The higher the Mach number, the more small

scale enhancements we expect to see.

As δ increases, differences between supersonic ($\mathcal{M}_s$= 3.0) and very supersonic ($\mathcal{M}_s$= 8.0) cases become more apparent, as the slopes for the $\mathcal{M}_s$= 3.0 case are steeper. This is because interacting shocks in the $\mathcal{M}_s$= 8.0 are much stronger, and hence there is more contrast in the emission contours. Thus, as we increase δ, the structures merge more rapidly for lower values of the sonic Mach number.

Comparison between the left and right panels shows that the magnetic field also affects the number of structures and the trend with the threshold value. When δ is low (i.e. there is more structure in the tree) the low magnetized case (super-Alfvénic, right panel) shows slightly more structures then the highly magnetized case. However, as the threshold value increases, the number of structures decreases more rapidly in the case of the super-Alfvénic case, which is evident in that the slopes are steeper regardless of the sonic Mach number. These trends with magnetic field are due to differences between MHD and hydrodynamic turbulence. For super-Alfvénic gas (which is close to hydrodynamic), turbulent eddies can evolve with a full 3D range of motion and have more degrees of freedom then plasma turbulence in the presence of a strong magnetic field. For turbulence in the sub-Alfvénic regime, the strong field creates anisotropy in the eddies, which are stretched along the direction of the mean field line. This limits the range of motion of the eddies which in turn, limits their ability to interact. Structures in the supersonic sub-Alfvénic cases show more contrast in PPV, meaning that the local maximum are generally higher and differences from the mean are more pronounced (this will be discussed more in the next subsection with the moments). Hence, as we increase δ, the structures in sub-Alfvénic turbulence do not merge with each other as quickly as in the case of the super-Alfvénic turbulence, which has less contrast in its emission cubes.

In light of this, we might also expect the structures in sub-Alfvénic turbulence to show less hierarchical structure overall. A test of hierarchy is to count the number of segments along the largest branch, from leaf to root. The bottom plot of Figure 4 shows the number of segments from root to leaf on the largest branch vs. the threshold parameter δ. Similar to what was shown in the top figure, the sonic Mach number has a strong relation to the amount of hierarchical structure created in the gas. Higher sonic Mach number yields more shocks which in turn produce more high density clumps and more hierarchical structures in PPV space. However, as expected from the top plot, the magnetic field seems to also play a strong role in the hierarchical branching. Comparison between the y-axis values of the left and right plots reveals that a larger Alfvénic Mach number creates more hierarchical structure in the PPV dendrogram. In the case of super-Alfvenic turbulence, magnetization is low and hence the structures created are closer to that of hydrodynamic turbulence, which is well known to show fractal behavior and hierarchical eddies. As turbulence transitions to sub-Alfvenic, it become magnetically dominated with fewer degrees of freedom. The contrast in sub-Alfvénic PPV data is higher, and hence there is less hierarchical structure as compared with super-Alfvénic turbulence.

We illustrate these findings in Figure 5. Case A shows a cloud with a global Alfvénic Mach number ≥ 1 while cases B and C show the same cloud with global Alfvénic Mach number ≤ 1 but with compression parallel and perpendicular to the field. All cases are assumed to have the same supersonic value of the sonic Mach number. Case A shows hierarchical structure forming in clumps that are not affected strongly by the magnetic field. The clumping and hierarchy is due to compression via shocks and the shredding effect of hydrodynamic turbulence. For case B and C, we now consider how this picture changes if we introduce a strong magnetic field. For shock compression parallel to the field lines (Case B), the clumps will be confined in the direction perpendicular to the field, and thus the compression will squeeze the clumps, decrease the hierarchy in the gas, create additional large density contrast. For shock compression perpendicular to the field lines, in this case the magnetic pressure relative to the shock compression is much higher, and the clumps will not feel as much of the compression. Thus in case B and C, the contrast is higher while hierarchical structure is less.

These results have interesting implications for hierarchical structures in interstellar and star forming clouds, which we will discuss more in the discussion section (section 7).

The plots in Figure 4 are for PPV cubes with LOS taken perpendicular to the mean magnetic field. We tested our results for LOS taken parallel to the mean magnetic field and found similar results.

4.1.2. *Statistics of the Dendrogram Distribution*

A dendrogram is a useful representation of PPV data in part because there are multiple ways of exploring the information on the data hierarchy. In this section we investigate how the statistical moments of the distribution of the dendrogram tree (see bottom panels of Figure 3 for example) changes as we change the threshold parameter δ and how these changes depend on the compressibility and magnetization of turbulence. We consider a distribution ξ containing all leaves and merging contour values in a given dendrogram. The question that forms the basis of our investigation in this section is: Do the moments of the distribution ξ have any dependencies on the conditions of the gas (i.e. the sonic and Alfvénic Mach number) and how does this relate back to the previous subsection?

The 1st and 2nd order statistical moments (mean and variance) used here are defined as follows: $\mu_\xi = \frac{1}{N}\sum_{i=1}^{N}(\xi_i)$ and $\nu_\xi = \frac{1}{N-1}\sum_{i=1}^{N}\left(\xi_i - \overline{\xi}\right)^2$, respectively. The standard deviation is related to the variance as: $\sigma_\xi^2 = \nu_\xi$. The 3rd and 4th order moments (skewness and kurtosis) are defined as:

$$\gamma_\xi = \frac{1}{N}\sum_{i=1}^{N}\left(\frac{\xi_i - \mu_\xi}{\sigma_\xi}\right)^3 \tag{4}$$

$$\beta_\xi = \frac{1}{N}\sum_{i=1}^{N}\left(\frac{\xi_i - \mu_\xi}{\sigma_\xi}\right)^4 - 3 \tag{5}$$

We calculate the moments of the dendrogram tree distribution while varying our simulation parameter space.

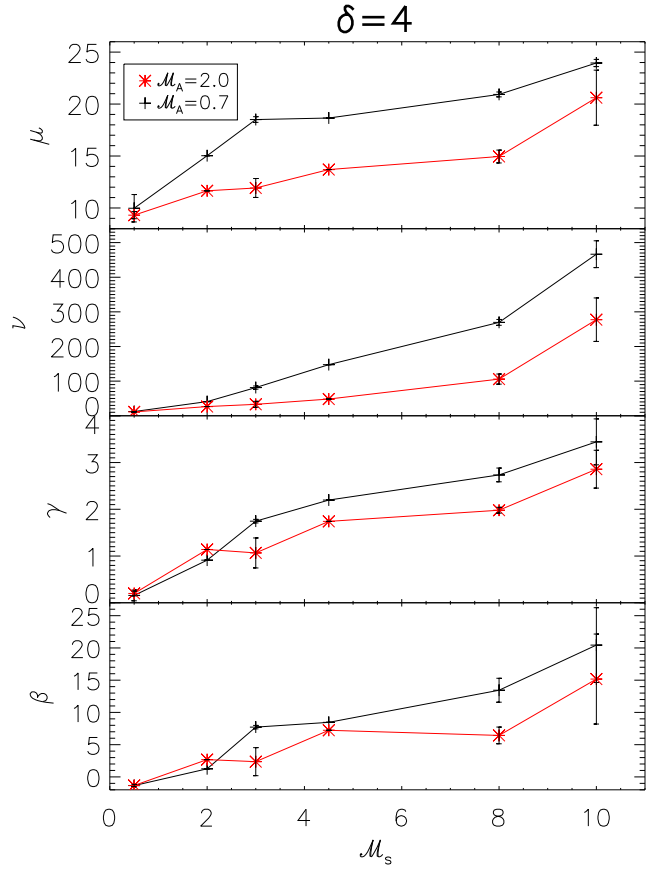

FIG. 6.— Moments of the dendrogram tree (leaves + branches) vs. $\mathcal{M}_s$ for twelve different simulations spanning a range of sonic numbers from 0.5 to 10. Here we have chosen δ=4. Panels show mean, variance, skewness and kurtosis of the distribution. Sub-Alfvénic is shown in black color and super-Alfvénic in red color.

In particular, we vary the sonic Mach number, the Alvénic Mach number, and the threshold value. We find the moments vs. the threshold parameter δ to show linear behavior. As δ increases, the number of the intermediate intensity values that make up the branches and the hierarchical nesting (i.e. the intensity values between the high intensity local maximum and the low intensity values near the trunk) merge with each other. This effect can be seen visually in Figure 3. Thus, as δ increases, the mean and variance of the distribution (example show in the bottom of Figure 3) will increase.

We plot the moments vs. $\mathcal{M}_s$ with $\delta = 4$ in Figure 6. This figure shows the full range of our simulations with sub- and super-Alfvénic combinations. Generally as the sonic Mach number increases so do the moments. We found this trend to be consistent over a range of δ values, and hence only plot one case here. Error bars, created by taking the standard deviation of the value between different time snapshots of the simulation, generally increase with sonic number as the fluctuations become increasingly stochastic and shock dominated. Physically, the increase of the moments of ξ is related to the compressibility of the model and more supersonic cases display more prominent clumpy features, which drive up the both the average and the variation from average. The tails and peak of the distribution also become increasingly skewed and kurtotic towards higher values of intensity and the distribution becomes more peaked around the mean value.

It is interesting to note that a strong dependency on the magnetization of the model exists, particularly as the sonic number goes up. The sub-Alfvénic simulations show increased moments, which implies that they exhibit more contrast (mean value is higher) and more skewed/kurtotic distributions in their gas densities. This result is to be expected based on the findings of the previous subsection, which showed sub-Alfvénic turbulence to exhibit less hierarchical nesting.

In the above analysis the distribution ξ included all leaves and branches of the dendrogram tree. We could further cut the tree into its respective branches and leaves and analyze the distributions separately, which provides additional constraints on the parameters. We investigated the statistical moments on the histograms of the branch lengths, leaf lengths, and leaf intensities and found the trends discussed above to be consistent with the results of Figure 6, and hence do not include the plots.

4.2. *Self-Gravity*

4.2.1. *Leaf and Branch Counting*

The issues of the importance of self-gravity in simulations have been raised by a number of authors (Padoan et al. 2001; Li et al. 2004; Goodman et al. 2009; Federrath et al. 2010). While self-gravity is known to be of great importance to accretion disk physics and protostellar collapse, its role in diffuse gasses is less obvious. As the dendrogram provides insight into the hierarchical structure of the PPV space, it can potentially be used to explore whether gravity has a major effect on both the structure of the hierarchy and the distribution of dominant emission contours.

Figure 7 shows the tree diagrams at constant δ=45 for super-Alfvénic supersonic simulations with different levels of self-gravity. This large value of δ is used in order to not over crowd the dendrogram with branches. We choose a super-Alfvénic model because super-Alfvénic supersonic turbulence is thought by many to be the type of conditions that exist in star forming molecular clouds (see Padoan & Nordlund 1999). In this figure, high gravity is $\approx$ 4 orders of magnitude larger then the weak gravity case. Gravity affects the dendrogram both in terms of structure and number of significant emission regions. Visually from Figure 7, one can see at constant δ, higher gravitational strength creates a dendrogram that has more hierarchical structures. We use a high value of δ to keep the plots from being over crowded with branches.

We show the number of structures vs. δ in Figure 8 using a logarithmic scale similar to the top of Figure 4. Our analysis spans the ranges of δ from 4-40. High and low levels of self-gravity with Alfvén number=2.0 and sonic number=7.0 and the corresponding no self gravity case are plotted in black, red, and blue, respectively. It is clear that the case with no self-gravity (symbolized with blue diamonds) shows less overall structure compared with the cases with self-gravity. High gravity simulations have significantly more nested structures and more contours considered to be areas of significant emission then low gravity. Interestingly, the power law behavior that is seen in the case with no gravity in Figure 8 and all of the cases in Figure 4 is absent for simulations with

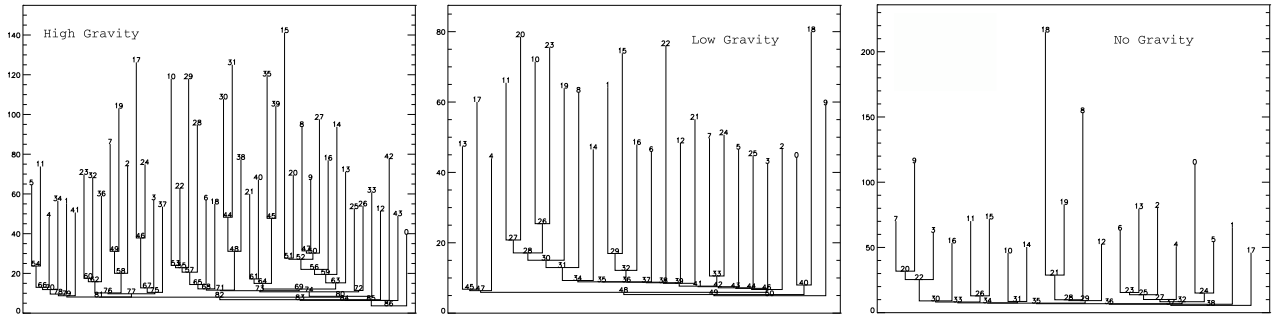

FIG. 7.— Effects of self-gravity on a 256^3 ideal MHD simulation with Alfvén number=2.0 and sonic number=7.0 with $\delta = 45$. A high value of δ is used to keep the plots from being over crowded with branches. The high self-gravity simulation is on the left, lower self-gravity in the center, and no gravity on the far right.

gravity. The absence of power-law behavior in the number of structures vs. δ may be used in ISM clouds to determine if self-gravity is important for cloud dynamics

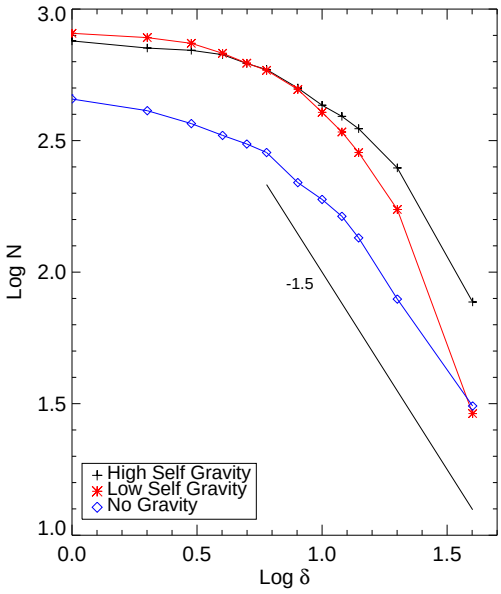

FIG. 8.— Total number of structures (branches and leaves) vs. δ on a log-log scale. Black plus signs indicated high gravity $\approx$ 4 orders of magnitude higher then the low gravity cases shown with red stars. Both of these have Alfvén number=2.0 and Sonic number=7.0. Comparison with a non self-gravitating simulation with Alfvén number=2.0 and sonic number=7.0 is shown with blue diamonds. We include a solid black line with slope=-1.5 to show the power-law nature of the non self-gravitating case.

4.2.2. *Statistics of the Dendrogram Distribution*

We show how self-gravity affects the dendrogram distribution as we vary δ in Figure 9 for a simulations with Alfvén number=2.0 and Sonic number=7.0. Higher levels of self-gravity show increases in all four moments over a range δ. The trends are smooth and linear as δ varies. The moments for this simulation with self-gravity are similar in magnitude to the case without self-gravity in the $\delta = 4$ example shown in Figure 6.

5. DENDROGRAMS OF PPP VS. PPV

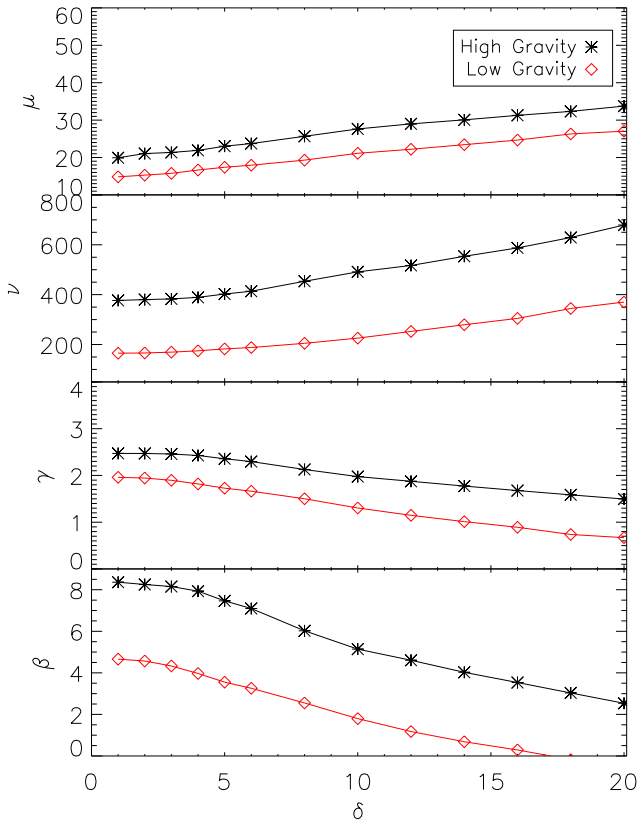

FIG. 9.— Moments of the dendrogram distribution vs. δ for models with self-gravity. High self-gravity (black lines) is 4x stronger then low self-gravity (red lines). Higher self-gravity shows increased amplitudes in the dendrogram (reflected in the mean), higher variance in values, and more skewed and peaked distributions, which are reflected in the skewness and kurtosis.

The issue of interpreting structures seen in PPV space has vexed researchers for over a decade (see Pichardo et al. 2000). How the structures in PPV translate to PPP depends on many factors, most importantly the nature of the turbulent environment. The dendrogram presents a unique way of studying how the hierarchy of structures seen in density space (PPP) relate to PPV space via simulations. From analyzing the spectrum of density and velocity with techniques such as VCS, one finds that the spectrum of PPV is dominated by density in

the case of supersonic turbulence while in the case of subsonic turbulence, velocity dominates. One might expect these signatures to also show up in a dendrogram analysis. This is useful for observers especially, since it is critical that they be able to interpret the morphologies observed in PPV space in a physically meaningful way.

For turbulent clouds, it is never the case that the structures in PPV have a one-to-one correspondence with the density PPP, although this assumption may be more appropriate for some environments then others. We show a simple example illustrating this in Figure 10 which shows synthetic PPV data cubes (left), and a PPP data cube (i.e. a density cube, right) for subsonic super-Alfvénic turbulence. The bottom left PPV cube has constant density/column density, while the top left PPV cube's corresponding density cube is shown on the right.

Interestingly, the bottom left PPV cube has a very similar level of structure to it as compared with the top PPV cube, despite the fact that the column density of the bottom cube is constant. This points out the well known fact that there is not a one-to-one correspondence with PPV and PPP space. In fact, in this example (a subsonic model) most of the structures are due to the velocity rather then the density. Figure 10 illustrates the dominance of velocity in the subsonic case in the bottom PPV cube. Fluctuations in PPV here are *entirely driven by the turbulent velocity field*.

To illuminate this point further Figure 11 shows PPP and PPV dendrograms for supersonic turbulence with $\mathcal{M}_s$=8.0 (middle) and subsonic turbulence with $\mathcal{M}_s$=0.5 (bottom). We also show the corresponding isosurfaces for the supersonic case in the top row. Comparing PPV and PPP should be done with care as they are different spaces. Here we increased the value of δ until the PPP dendrogram becomes mostly leaves, that is, they have little hierarchy. The leaves are reached at $\approx \delta = 40$. We took the corresponding optically thin PPV cube and applied the dendrogram with the same $\delta = 40$ threshold value. If the dominate emission is due to *density* then the leaves should be similar for both PPV and PPP. All PPV and PPP cubes have mean value of unity.

Interestingly, the supersonic turbulence dendrogram for density looks very similar to the corresponding PPV dendrogram for the same δ at the level of the leaves. For the subsonic case we see that the dendrogram of density and PPV look nothing alike (same δ). In this case, the velocity field dominates PPV space. Hence, we don't show the isosurfaces for the subsonic case. In supersonic turbulence, the highest density peaks correspond to the highest intensity fluctuation in the PPV. This implies that if one knows the turbulence in question is supersonic, the structures in PPV space at the level of the leaves can be generally interpreted as 3D density structures. However, if the turbulence is subsonic in nature, this assumption may not be appropriate.

6. APPLICATION

The different parts of the dendrogram tree show dependencies on parameters of turbulence that are particularly important to both studies of star forming regions and the diffuse ISM. When analyzing a particular data set, one should keep in mind that comparisons between the observational and scaled numerical data, or comparisons between different clouds or objects in the data are the most useful means of extracting these parameters.

Our simulations can be scaled to observations by specifying physical size of the simulation volume, the isothermal sound speed of the gas, and mass density. For example, the velocity scale factor v_0,which relates simulation velocities to physical velocities, is given by:

$$v_0 = Cs_{obs}/Cs_{sim} = cs_{obs}\sqrt{\rho_{sim}/P_{sim}} \qquad (6)$$

where Cs is the sound speed, P is the gas pressure, and ρ is the density. More information on scaling simulations to observations can be found in Hill et al. 2008

We include the effects of changing the velocity resolution, thermal broadening, and smoothing in the next subsection.

6.1. *Smoothing*

We investigate how smoothing and data resolution affect the dendrogram. When dealing with observational data one must always consider the effect that the telescope beam smoothing will have on the measurement. The observations are rarely done with pencil beams and the measured statistics change as the data is averaged. We expect the effect of smoothing to depend on a dimensionless number, namely, the ratio of the size of the turbulence injection scale to the smoothing scale.

We apply the same technique that was applied in the previous sections, i.e. exploring number of structures and moments of dendrogram tree statistics, however now we include a boxcar smoothing kernel (truncating the edges). We expect that smoothing will affect supersonic turbulence and cases of high self-gravity the most. In this case, shocks and small scale gravitational clumps become smoothed out and more difficult for the algorithm to identify. In the subsonic or low gravity cases, smoothing makes less of a difference since the gas is already diffuse and less hierarchical.

We show how the moments and number of structures changes with smoothing size (in pixels) in Figure 12. One could also discuss smoothing beam size in terms of the injection scale of the turbulence. For instance, 7 pixel smoothing represents a beam scale that is 30 times smaller then our injection scale of turbulence.

We found that generally, subsonic and transonic turbulence are not as affected by smoothing compared to highly supersonic models. In light of this, we plot the moments and number of structures vs. δ for different smoothing degrees for a highly supersonic model with $\mathcal{M}_s$=8.0 in Figure 12. Two panels show different Alfvénic regimes with the y-axis the same for both for ease of comparison. Black lines indicate no smoothing, while red and blue indicate three and seven pixel smoothing, respectively. Error bars are produced by taking the standard deviation between different time snapshots of the simulations with well developed turbulence.

As smoothing increases for this supersonic model, we see that the values of the moments as well as the total number of structures decreases. However, even out to seven pixel smoothing the differences between the Aflvénic cases is evident in the mean and variance, respective of the error bars. Furthermore, the trends with the threshold parameter do not change when we introduce smoothing, which gives us further confidence that this technique can be applied to the observational data.

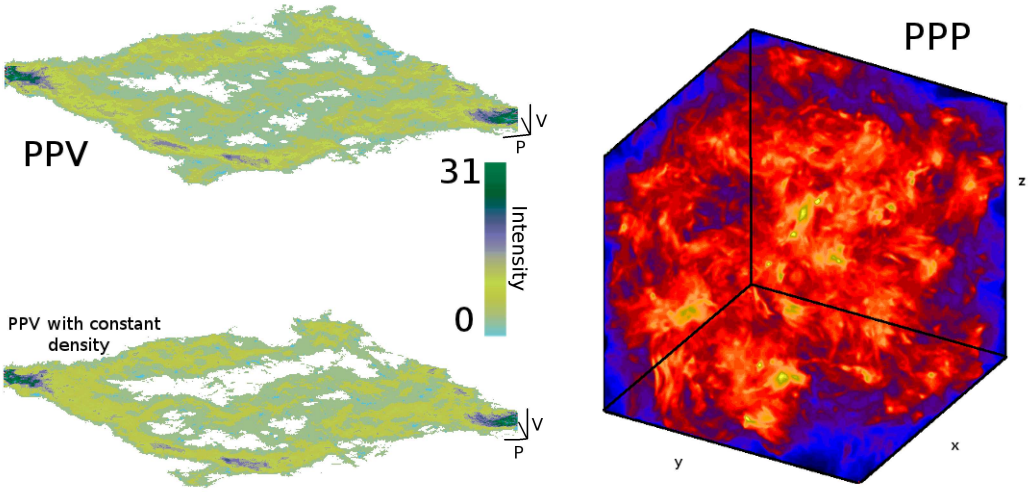

FIG. 10.— Example of a synthetic PPV data cubes with vertical axis being the velocity axis (left), and PPP data cube (right) for subsonic super-Alfvénic turbulence. Integrating along the velocity axis of PPV restores the column density map which can also be obtained from the 3D density cube. The bottom left PPV has PPP density equal to unity, and hence a constant column density. Structure in this PPV cube is due to *pure velocity fluctuations*, yet it still shows structure. This figure highlights the need to be cautious when translating the structures seen in PPV to PPP. The quantitative relation between the fluctuations in PPV and underlying density and velocity fluctuations is provided in Lazarian & Pogosyan (2000)

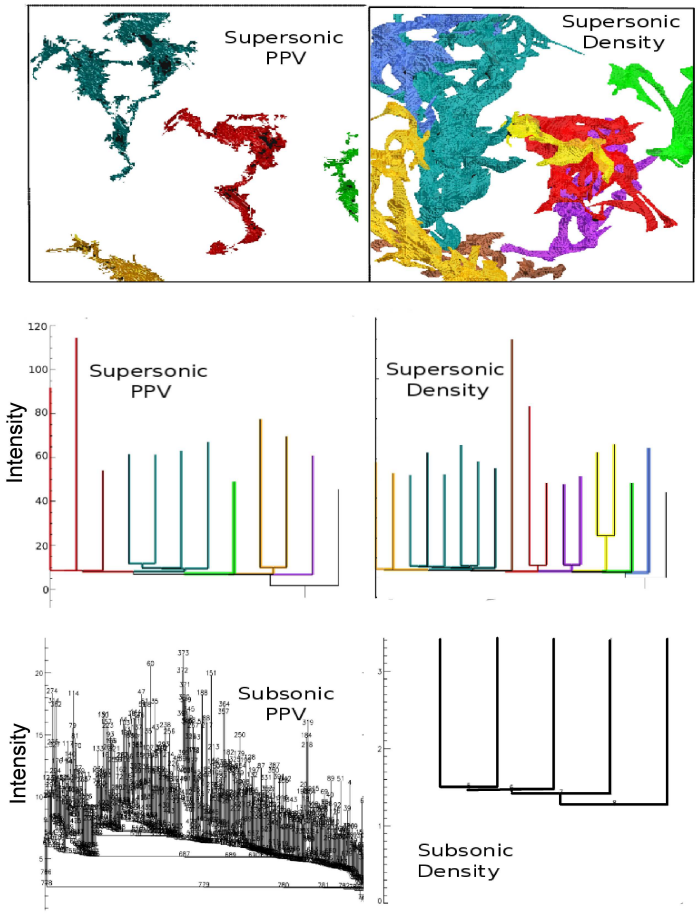

FIG. 11.— Dendrograms of density (right column) and PPV (left column). Supersonic isosurfaces and their corresponding dendrograms are shown in the top and middle rows. Colors are correspondent between structures in the isosurface figures and the dendrogram. Subsonic dendrograms are shown in the bottom row.

Other than the change in amplitude, the trends remain the same as what was seen in Section 4.

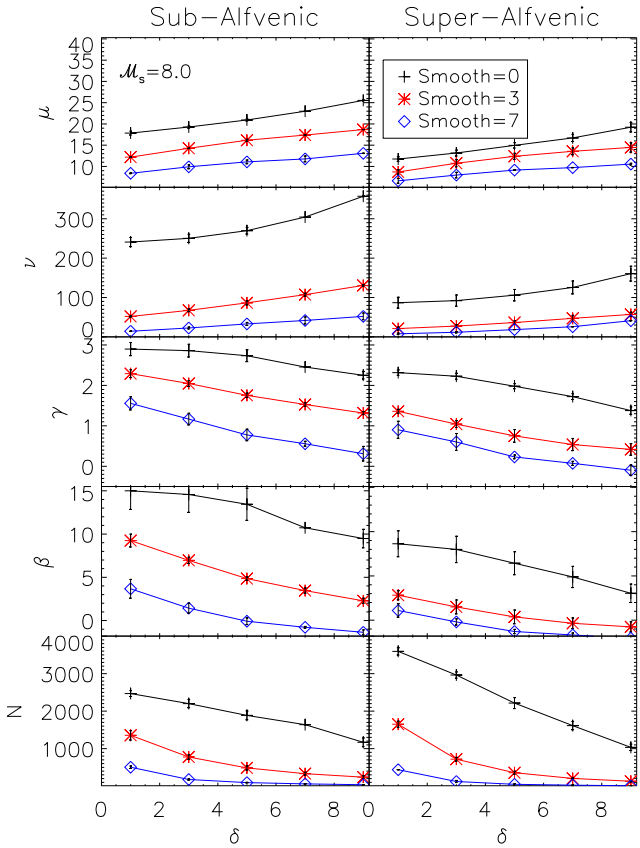

FIG. 12.— Change in the moments dendrogram distribution and the number of structures with smoothing vs. the threshold parameter δ . The left panel is sub-Alfvénic and the right panel is super-Alfvénic and the y-axis is the same for both columns for ease of comparison between the two. Both cases have $\mathcal{M}_s$=8.0.

6.2. *Velocity Resolution*

In addition to smoothing we must also consider the effects of velocity resolution. As the velocity resolution

changes in PPV space, so do the structures observed. We investigated how the moments of the dendrogram branch + leaf distribution changed when we vary the velocity resolution. We find that the number of substructures drops dramatically as the velocity resolution decreases, from several hundreds to several dozen when changing the velocity resolution from $v_{res} = 0.07$ to $v_{res} = 0.7$. This effect corresponds to the channel sampling dropping from ≈ 60 down to 15 channels. This may provide too low a number of statistics in the dendrogram distribution to look at the moments, however the general trends with the physical parameters stay consistent with section 4. The same holds for the case where we increase the velocity resolution an order of magnitude (up to $v_{res} = 0.007$).

6.3. *Thermal Broadening*

The bulk of this paper focuses on the effects of turbulence and magnetic fields in the creation of hierarchical structure in ISM clouds, however thermal broadening effects must also be considered as well. Convolution with a thermal broadening profile (i.e. a Gaussian) will smooth out the velocity profiles and generally decrease the intensities. We convolve the line profiles of eight of our simulations with sonic Mach numbers ranging from $\mathcal{M}_s$=2.0-10 with Gaussian profiles to mimic the effects of thermal broadening. The thermal Gaussian has FWHM given as the ratio of the turbulent line width to the sonic Mach number. As thermal broadening will change the intensity range of our simulations, we accordingly change the values of the threshold parameter δ. We scale δ down from the range used in Section 4 by a factor of $< PPV_{thermal+turbulent} > / < PPV_{turbulent} >$, in order to fully sample how the contours merge in the new cubes.

We show the effects of including thermal broadening on the number of structures and amount of hierarchical structure in Figure 13. While the threshold value had to be lowered due to the intensity change in the PPV cubes, the trends are similar to those presented in Section 4 when thermal broadening was not included. Namely, that supersonic super-Alfvénic turbulence generally shows more overall structure and more hierarchical structure. The main difference seen with the inclusion of thermal broadening is that the slopes of the power law trends of log N vs. log δ are shallower in all cases. The slopes for the sub-Alfvénic panel are -1.6, -1.2, -0.48, -0.2 for $\mathcal{M}_s$=2.0, 3.0, 8.0 and 10, respectively. The slopes for the super-Alfvénic panel are -1.8, -1.7, -0.7, -0.25 for $\mathcal{M}_s$=2.0, 3.0, 8.0 and 10, respectively. For reference the slopes for $\mathcal{M}_s$=3.0 and 8.0 from Figure 4 were -2.2 and -1.1, respectively for sub-Alfvénic turbulence and -3.3 and -1.67 for super-Alfvénic turbulence.

Similarly to Figure 4, the super-Alfvénic slopes remain steeper then the sub-Alfvénic. This shows that the effects seen in the previous sections are due primarily to the level of turbulence and the Alfvénic Mach number in the simulations, and are not masked over with thermal broadening.

7. DISCUSSION

Hierarchical tree diagrams are finding more applications in interstellar studies, not only to locate clumps and calculate their properties, but also for characterizing properties of the physics present in interstellar and molecular gas. In this paper we used dendrograms to analyze how turbulence, magnetic fields and self-gravity shape the amount of structure and gas hierarchy in isothermal simulations. We also examined the changes in the distribution of the dendrogram as we vary the threshold parameter δ. This is analogous to changing the corresponding threshold parameter in other techniques that rely on contouring thresholds, e.g. in the Genus analysis (see Chepurnov et al. 2009). By varying δ we obtained a new outlook on the technique; in particular, we found that the dendrogram distribution and hierarchy have a strong dependency on the magnetization and compressibility of the gas and are sensitive to the amount of self-gravity.

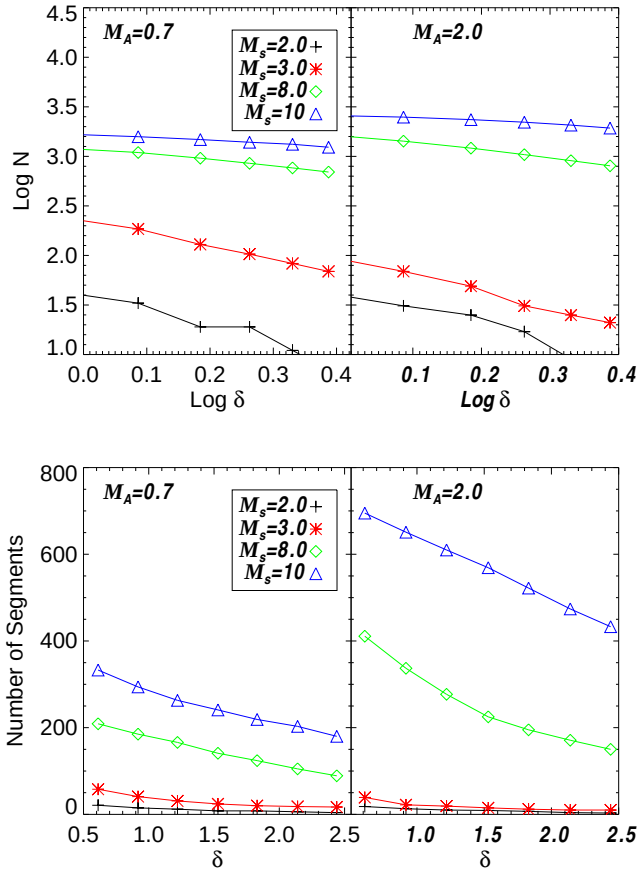

FIG. 13.— Top: Total number of structures (leaves and branches) vs. δ. Bottom: Number of segments from root to leaf on the largest branch of the tree vs. δ. Both plots are similar to Figure 4, only here we include the effects of thermal broadening. In both top and bottom plots the left panel is shows higher magnetization (sub-Alfvénic) while the right shows lower magnetization (super-Alfvénic). Both panels have the y-axis set to the same range for ease of comparison. Hierarchical structure and overall structure is created both by shocks and a high Alfvénic Mach number, even when thermal broadening effects are included.

7.1. *The Hierarchical Nature of MHD Turbulence*

The number of structures and the amount of hierarchy formed by MHD turbulence has interesting implications for the evolution of ISM clouds and for the star formation problem. In section 4 we found that more hierarchical structure and more overall structure was created in the presence of supersonic super-Alfvénic turbulence. We also found that the inclusion of self-gravity enhanced

these trends. The relationship between the magnetization and the cloud dynamics is in the process of being understood, especially in regards to star formation. Star forming clouds are known to be hierarchical in nature and magnetized, but the exact Alfvénic nature is less clear. The results from this work seem to suggest that very hierarchical clouds might tend towards being super-Alfvénic. Several authors have suggested a variety of evidence for molecular clouds being super-Alfvénic. This includes the agreement of simulations and observations of Zeeman-splitting measurements, B vs.ρ relations, $\mathcal{M}_A$ vs. ρ relations, statistics of the extinction measurement etc. (Padoan & Nordlund 1999; Lunttila et al. 2008; Burkhart et al. 2009; Crutcher et al. 2009; Collins et al. 2012). Furthermore a study done by Burkhart et al. 2009 found that, even in the presence of globally sub-Alfvénic turbulence, the highest density regions tend towards being locally super-Alfvénic. This suggests that even in the case of globally sub-Alfvénic turbulence, the densest regions might be super-Alfvénic. It is interesting that the dendrogram technique also points to super-Alfvénic turbulence as an avenue for hierarchical structure creation. This provides motivation for the dendrogram technique to be applied to the observational data with varying threshold value δ in order to see how the nature of the hierarchical structure and total number of structures change in the observations.

7.2. *Sonic and Alfvénic Mach Numbers from the Observations*

In the paper above we provided a systematic study of the variations of the dendrogram δ with the sonic and magnetic Mach numbers. These numbers are critical for understanding most of processes in galactic diffuse and molecular gas, including the process of star formation. Thus, the dendrogram provides an avenue of obtaining these parameters via comparing observations and simulations and/or as a technique for investigating what processes are creating hierarchical structure in ISM gas.

We view this work as the springboard for applying the technique to the actual data. We claim that for reliable studies of the interstellar media and molecular clouds it is most advantageous to combine different techniques. For instance, applying the VCA and VCS techniques to PPV data (see Lazarian 2009 for a review), one can obtain the velocity and density spectra of turbulence. While these measures are known to depend on $\mathcal{M}_s$ and to a lesser degree on $\mathcal{M}_A$ (see Beresnyak, Lazarian & Cho 2005, Kowal et al. 2007, Burkhart et al. 2009), the utility of the spectra is not in measuring these quantities. Spectra provide a unique way to investigate how the energy cascades between different scales, and shows whether comparing observations with the simulations with a single scale of injection is reasonable.

The analysis of the anisotropies of correlations using velocity centroids provides an insight into media magnetization, i.e., provides $\mathcal{M}_A$ (Lazarian et al. 2002, Esquivel & Lazarian 2005), which is complimentary to the technique described in this paper. Studies of the skewness and kurtosis of the PDFs (see Kowal et al. 2007, Burkhart et al. 2009, 2010) provides measures of the sonic Mach number $\mathcal{M}_s$. Similarly, Tsallis statistics measures (Esquivel & Lazarian 2010, Tofflemire et al. 2011) provide additional ways of estimating both $\mathcal{M}_s$ and $\mathcal{M}_A$. We feel the approach to obtaining these parameters should be conducted with synergetic use of multiple tools, such as was done in Burkhart et al. 2010 on the SMC. We feel the dendrogram is a unique tool as it can classify the hierarchical nature of the data and that it should be added to a standard set of statistical-tools for studies of ISM data.

All these techniques provide independent ways of evaluating parameters of turbulence and therefore their application to the same data set provides a more reliable estimate of key parameters such as compressibility, magnetization, and degree of self-gravity. Dendrograms have some advantages over other statistics designed to search for turbulence parameters, in that one can analyze the resulting tree diagram in many different ways, as highlighted in this paper and in previous works. These include finding local maxima, calculating physical properties of dominate emission, exploring how those clumps are connected in PPV, varying the threshold and calculating moments and level of hierarchy. Of course, one should keep in mind that the medium that we investigate observationally is far from simple. Multiple energy injection sources, for example, are not excluded. Thus obtaining a similar answer with different techniques should provide us with additional confidence in our results.

Finally, we should stress, that for studies of astrophysical objects the dendrogram and other statistical measures can be applied locally to different parts of the media. For instance, Burkhart et al. (2010) did not characterize the entire SMC with one sonic Mach number. Instead, several measures were applied to parts of the SMC in order to obtain a distribution of the turbulence in the galaxy. A similar local scale selection was applied also to the SMC in Chepurnov et al. (2008) using the Genus technique. The same technique should be used to parts of the ISM in the Milky way and may be attempted for GMCs. Correlating the variations of the turbulence properties with observed properties of the media, e.g. star formation rate should provide insight into how turbulence regulates many key astrophysical processes.

8. SUMMARY

We apply dendrograms to isothermal MHD simulations with varying levels of gravity, compressibility and magnetization. We find that the dendrogram is a promising tool for studying both gas connectivity in the ISM as well as characterizing turbulence. In particular we find that:

- We propose using statistical descriptions of dendrograms as a means to quantify the degree of hierarchy present in a PPV data cube.
- Shocks, self-gravity, and super-Alfvénic turbulence create the most hierarchical structure in PPV space.
- The number of dendrogram structures depends primarily on the sonic number and the level of self-gravity and secondarily on the global magnetization.
- The first four statistical moments of the distribution of dendrogram leaves and connecting have monotonic dependencies on the level of self-gravity and the sonic and Alfvén Mach numbers over a range of δ.

- The dendrogram provides a convenient way of comparing PPP to PPV in simulations. Density structures are dominant in supersonic PPV and not in subsonic. Thus it is more justifiable to compare PPV directly to PPP when the gas is known to be supersonic.

B.B. acknowledges support from the NSF Graduate Research Fellowship and the NASA Wisconsin Space Grant Institution. B.B. is thankful for valuable discussions and the use of the Dendrogui code via Chris Beaumont. A.L. thanks NSF AST 0808118, the Center for Magnetic Self-Organization in Astrophysical and Laboratory Plasmas for financial support. This work was completed during the stay of A.L. as Alexander-von-Humboldt-Preisträger at the Ruhr-University Bochum. A.G. acknowledges support from NSF Grant No. AST-0908159. E.R. is supported by a Discovery Grant from NSERC of Canada.

REFERENCES

Armstrong,J. W., Rickett, B. J., Spangler, S. R., 1995, ApJ, 443, 209
Ballesteros-Paredes, J., Klessen, R. S., Mac Low, M.-M., & Vazquez-Semadeni, E. 2007, in Protostars and Planets V, ed. B. Reipurth, D. Jewitt, & K. Keil (Tucson, AZ: Univ. of Arizona Press), 63
Beresnyak, A., Lazarian, A., Cho, J., 2005, ApJ, 624, 93
Berkhuijsen E., Fletcher, A., 2008, MNRAS, 390, 19
Brunt, C. M., Kerton, C. R., & Pomerleau, C., 2003, ApJS, 144, 47
Brunt, C., & Heyer, M., 2002, ApJ, 566, 27
Brunt, C., 2010, A&A, 513, 67
Burkhart, B., Falceta-Goncalves, D., Kowal, G., Lazarian, A., 2009, ApJ, 693, 250
Burkhart, B., Stanimirovic, S., Lazarian, A., Grzegorz, K., 2010, ApJ, 708, 1204
Burkhart, B., Lazarian, A., Gaensler, B., 2012, ApJ, 708, 1204
Burkhart, B., & Lazarian, A., 2011, IAUS, 274, 365
Chepurnov, A., Gordon, J., Lazarian, A., & Stanimirovic, S.,2008, ApJ, 688, 1021
Chepurnov, A., & Lazarian, A. 2009, ApJ, 693, 1074
Chepurnov & Lazarian, 2010, ApJ, 710, 853
Cho, J. & Lazarian, A. 2003, MNRAS, 345, 325
Collins et al., 2012, ApJ, 750, 13
Crutcher, R., Hakobian, N., Troland, T., 2009, ApJ, 692, 844
Elmegreen, B. G., & Elmegreen, D. M. 1983, MNRAS, 203, 31
Elmegreen, B. G., & Scalo, J. 2004, ARA&A, 42, 211
Elmegreen, B. G., 2011, Star Formation in the Local Universe, Eds. C. Charbonnel & T. Montmerle, EAS Publications Series
Esquivel, A, & Lazarian, A., 2005, ApJ, 295,479
Esquivel, A., & Lazarian, A., 2010, ApJ, 710, 125
Falgarone, E., Lis, D. C., Phillips, T. G., Pouquet, A., Porter, D. H., & Woodward, P. R. 1994, ApJ, 436, 728
Ferriere, K., 2001, RvMP, 73, 1031
Federrath, C., et al., 2008, ApJ, 688, 79
Federrath, C., et al., 2010, ApJ, 713, 269
Feitzinger, J. V., & Galinski, T. 1987, A&A, 179, 249
Frisch, U., 1995, Turbulence, Univ. of Cambridge Press
Gaensler et al., 2011, Nature, 478, 214-217
Gill, A.G., & Henriksen, R.N., 1990, ApJ, 365, L27
Goodman et al., 2009, Nature, 457, 63
Goodman, A., Pineda, J., Schnee S., 2009, ApJ, 692, 91
Haverkorn, M., & Heitsch, F., 2004, A&A,421, 1011
Hill, A. et al., 2008, ApJ, 686, 363
Houlahan P., & Scalo J., 1992, ApJ, 393, 172
Kang, H., Ryu, D., & Jones, T. W., 2009, ApJ, 695, 1273
Kainulainen, J., Beuther, H., Banerjee, R., Federrath, C., Henning, T., 2011, A&A, 530, 64
Kim, S., Park, G., 2007, ApJ, 663, 244
Kowal, G., Lazarian, A. & Beresnyak, A., 2007, ApJ, 658, 423
Larson, R.B. 1981, MNRAS, 194, 809
Lazarian, A., 2004, J. Korean Astron. Soc., 37, 563
Lazarian, A., 2009, SSR, 143, 357
Lazarian A., & Esquivel, A., 2003, ApJ, 592, 37
Lazarian, A. & Pogosyan,D., 2000, ApJ, 537, 720
Lazarian, A. & Pogosyan, D., 2004, ApJ, 616, 943
Lazarian,A. & Pogosyan,D., 2006,ApJ, 652, 1348
Lazarian, A. & Pogosyan,D., 2008,ApJ, 686, 350
Lazarian, A., Pogosyan, D., & Esquivel, A. 2002, in ASP Conf. Proc. 276, Seeing Through the Dust: The Detection of H I and the Exploration of the ISM in Galaxies, ed. A. R. Taylor, T. L. Landecker, & A. G. Willis (San Francisco: ASP), 182
Li, P. S., Normand, M., Mac Low, M., Heitsch, F., 2004, ApJ, 605, 800
McKee, C., Ostriker, E., 2007, , ARA&A, 45, 565
Ossenkopf, V., & Mac Low, M.-M., 2002, A&A, 390, 307
Ossenkopf, V., Esquivel, A., Lazarian, A., & Stutzki, J. 2006, A&A, 452, 223
Ostriker, E., Gammie, C., Stone, J., 1999, ApJ, 513, 259
Padoan, P., & Nordlund, A., 1999, ApJ, 526, 27
Padoan, P., Rosolowsky, E. W., & Goodman, A. A. 2001, ApJ, 547, 862
Padoan, P., Nordlund, A., Rognvaldsson, O. E., & Goodman, A. A., 2001, in ASP Conf. Ser. 243, From Darkness to Light: Origin and Evolution of Young Stellar Clusters, ed. T. Montmerle, & P. Andre (San Francisco: ASP), 279
Padoan, P., Goodman, A., Juvela, Mika, 2003, ApJ, 588, 881
Padoan, P., Juvela, M., Kritsuk, A. G., & Norman, M. L. 2009, ApJ, 707, L153
Pichardo et al. 2000, ApJ, 532, 353
Podani, J., Engloner, A., & Major, A., 2009, Stat. Appl. Genet. Mol. Biol., 22.
Price, Federrath, & Brunt, 2011, ApJ, 727
Rosolowsky, E., Goodman, A., Wilner, D., Williams, J.,1999, ApJ, 524, 887
Rosolowsky, E., & Blitz, L., 2005, ApJ, 623, 826
Rosolowsky, E. W., Pineda, J. E., Kauffmann, J., & Goodman, A. A. 2008, ApJ, 679, 1338
Sawlaw W. & Haque-Copilah, S., 1998, ApJ 509, 595
Spangler, S. R., & Gwinn, C. R. 1990, ApJ, 353, L29
Toffelmire, B., Burkhart, B., Lazarian, A., 2011, ApJ, 736, 60
Scalo, J.S. 1985, in Protostars and Planets II, ed. D.C Black and M. S. Matthews, (Tucson: Univ. of Arizona Press), p. 201
Scalo, J. 1990, in Physical Processes in Fragmentation and Star Formation, eds. R. Capuzzo-Dolcetta, C. Chiosi, & A. Di Fazio, Dordrecht: Kluwer, p. 151
Stutzki, J., Bensch, F., Heithausen, A., Ossenkopf, V., Zielinsky, M., 1998, A&A, 336,697
Vazquez-Semadeni, E., 1993, ApJ, 423, 681

Hierarchical Structure of Magnetohydrodynamic Turbulence In Position-Position-Velocity Space

Blakesley Burkhart[1], A. Lazarian[1], Alyssa Goodman[2], Erik Rosolowsky[3]

ABSTRACT

Magnetohydrodynamic turbulence is able to create hierarchical structures in the interstellar medium that are correlated on a wide range of scales via the energy cascade. We use hierarchical tree diagrams known as dendrograms to characterize structures in synthetic Position-Position-Velocity (PPV) emission cubes of optically thin isothermal magnetohydrodynamic turbulence. We show that the structures and degree of hierarchy observed in PPV space are related to the physics of the gas, i.e. self-gravity and the global sonic and Alfvénic Mach number. Simulations with higher Alfvénic Mach number, self-gravity and supersonic flows display enhanced hierarchical structure. We observed a strong sonic and Alfvénic dependency when we apply the the statistical moments (i.e. mean, variance, skewness, kurtosis) to the dendrogram distribution. Larger magnetic field and sonic Mach number correspond to larger values of the moments. Application of the dendrogram to 3D density cubes, also known as Position-Position-Position cubes (PPP), reveals that the dominant emission contours in PPP and PPV are related for supersonic gas but not for subsonic. We also explore the effects of smoothing, thermal broadening and velocity resolution on the dendrograms in order to make our study more applicable to observational data. These results all point to hierarchical tree diagrams as being a promising additional tool for studying ISM turbulence and star forming regions in the direction of obtaining information on the degree of self-gravity, the Mach numbers and the complicated relationship between PPV and PPP.

Subject headings: ISM: structure — MHD — turbulence

[1]Astronomy Department, University of Wisconsin, Madison, 475 N. Charter St., WI 53711, USA

[2] Harvard-Smithsonian Center for Astrophysics, 60 Garden Street, MS-78, Cambridge, MA 02138

[3]University of British Columbia, Okanagan Campus,3333 University Way, Kelowna BC V1V 1V7, Canada

1. Introduction

The current understanding of the interstellar medium (ISM) is that it is a multi-phase environment composed of a tenuous plasma, consisting of gas and dust, which is both magnetized and highly turbulent (Ferriere 2001; McKee & Ostriker 2007). In particular, magnetohydrodynamic (MHD) turbulence is essential to many astrophysical phenomena such as star formation, cosmic ray dispersion, and many transport processes. (see Elmegreen & Scalo 2004; Ballesteros-Paredes et al. 2007 and references therein). Additionally, turbulence has the unique ability to transfer energy over scales ranging from kiloparsecs down to the proton gyroradius. This is critical for the ISM, as it explains how energy is distributed from large to small spatial scales in the Galaxy.

Observationally, several techniques exist to study MHD turbulence in different ISM phases. Many of these techniques focus on the density fluctuations in ionized media (Armstrong et al. 1995; Chepurnov & Lazarian 2010), fluctuations in spectroscopic data and column density maps for neutral media (Spangler & Gwinn 1990; Padoan et al. 2003) , or gradients of linear polarization maps (Haverkorn & Heitsch 2004; Gaensler et al. 2011; Burkhart, Lazarian & Gaensler 2012). For studies of turbulence, spectroscopic data has a clear advantage in that it contains information about the turbulent velocity field as well as the density fluctuations. However, density and velocity are entangled in PPV space, making the interpretation of this type of data difficult. For the separation of the density and velocity fluctuations, special techniques such as the Velocity Coordinate Spectrum (VCS) and the Velocity Channel Analysis (VCA) have been developed (Lazarian & Pogosyan 2000, 2004, 2006, 2008).

Most of the efforts to relate observations and simulations of magnetized turbulence are based on obtaining the spectral index (i.e. the log-log slope of the power spectrum) of either the density and/or velocity (Lazarian & Esquivel 2003; Esquivel & Lazarian 2005; Ossenkopf et al. 2006). However, the power spectrum alone does not provide a full description of turbulence, as it only contains the Fourier amplitudes and neglects information on phases. This fact combined with the knowledge that astrophysical turbulence is complex, with multiple injection scales occurring in a multiphase medium, points to researchers needing additional ways of analyzing observational and numerical data in the context of turbulence. In particular these technique studies are currently focused into two categories:

- Development: Test and develop techniques that will complement and build off of the theoretical and practical picture of a turbulent ISM that the power spectrum presents.
- Synergy: Use several techniques simultaneously to obtain an accurate picture of the parameters of turbulence in the observations.

In regards to the first point, there has been substantial progress in the development of techniques to study turbulence in the last decade. Techniques for the study of turbulence can be tested empirically using parameter studies of numerical simulations or with the aid of analytical predictions (as was done in the case of VCA). In the former, the parameters to be varied (see Burkhart & Lazarian 2011) include the Reynolds number, sonic and Alfvénic Mach number, injection scale, equation of state, and, for studies of molecular clouds, should include radiative transfer and self-gravity (see Ossenkopf 2002; Padoan et al. 2003; Goodman et al. 2009). Some recently developed techniques include the application of probability distribution functions (PDFs), wavelets, spectral correlation function (SCF),[1] delta-variance, the principal component analysis, higher order moments, Genus, Tsallis statistics, spectrum and bispectrum (Gill & Henriksen 1990; Stutzki et al. 1998; Rosolowsky et al. 1999; Brunt & Heyer 2002; Kowal, Lazarian & Beresnyak 2007; Chepurnov et al. 2008; Burkhart et al. 2009; Esquivel & Lazarian 2010; Tofflemire et al. 2011). Additionally, these techniques are being tested and applied to different wavelengths and types of data. For example, the PDFs and their mathematical descriptors have been applied to the *observations* in the context of turbulence in numerous works using different data sets including: linear polarization data (see Gaensler et al. 2011; Burkhart, Lazarian, & Gaensler 2012), HI column density of the SMC (Burkhart et al. 2010), molecular/ dust extinction maps (Goodman, Pineda, & Schnee 2009; Brunt 2010; Kainulainen et al. 2011) and emission measure and volume averaged density in diffuse ionized gas (Hill et al. 2008; Berkhuijsen & Fletcher 2008).

The latter point in regard to the synergetic use of tools for ISM turbulence is only recently being attempted as many techniques are still in the stages of being developed. However, this approach was used in Burkhart et al. 2010, which applied spectrum, bispectrum and higher order moments to H I column density of the SMC. The consistency of results obtained with a variety of statistics and compared with more traditional observational methods made this study of turbulence in the SMC a promising first step.

This paper falls under the category of "technique development." In particular, we investigate the utility of dendrograms in studying the hierarchical structure of ISM clouds. It has long been known that turbulence is able to create hierarchical structures in the ISM (Scalo 1985, 1990; Vazquez-Semadeni 1993 ;Stutzki 1998), however many questions remain, such as what type of turbulence is behind the creation of this hierarchy and what is the role of self-gravity and magnetic fields? Hierarchical structure in relation to these questions is particularly important for the star formation problem (Larson 1981; Elmegreen & Elmegreen 1983; Feitzinger & Galinski 1987; Elmegreen 2011).

[1]The similarities between VCA and SCF are discussed in Lazarian (2009).

The earliest attempts to characterize ISM hierarchy utilized tree diagrams as a mechanism for reducing the data down to hierarchical 'skeleton images' (see Houlahan & Scalo 1992). More recently dendrograms have been used on ISM data in order to characterize self-gravitating structures in star forming molecular clouds (Rosolowsky et al. 2008 and Goodman et al. 2009). A dendrogram (from the Greek dendron "tree",- gramma "drawing") is a hierarchical tree diagram that has been used extensively in other fields, particularly in computational biology, and occasionally in galaxy evolution (see Sawlaw & Haque-Copilah 1998 and Podani, Engloner, & Major 2009 for examples). Rosolowsky et al. (2008) and Goodman et al. (2009) used the dendrogram on spectral line data of L1448 to estimate key physical properties associated with isosurfaces of local emission maxima such as radius, velocity dispersion, and luminosity. These works provided a new and promising way of characterizing self-gravitating structures and properties of molecular clouds through the application of dendrogram to ^{13}CO(J=1-0) PPV data.

In this paper we apply the dendrogram to synthetic observations (specifically PPV cubes) of isothermal MHD turbulence in order to investigate the physical mechanisms behind the gas hierarchy. Additionally, we are interested in the nature of the structures that are found in PPV data and how these structures are related to both the physics of the gas and the underlying density and velocity fluctuations generated by turbulence. Simulations provide an excellent testing ground for this problem, as one can identify which features in PPV space are density features and which are caused by velocity crowding. Furthermore, one can answer the question of under what conditions do the features in PPV relate back to the 3D density or PPP cube?

In order to answer these questions we perform a parameter study using the dendrogram. We focus on how changing the global parameters of the turbulence, such as the sonic Mach number, Alfvénic Mach number and level of self-gravity affect the amount of hierarchy observed, the relationship between the density and velocity structures in PPV, and the number and statistical distribution of dominate emission structures. Along with the Reynolds number, the sonic and Alfvénic Mach numbers are useful descriptors of the turbulence and are critical to several phenomena in astrophysics, including cosmic ray acceleration, turbulent magnetic reconnection, ambipolar diffusion and structure formation in the ISM. They are defined as the ratio of the flow velocity to the sound speed and Alfvén speed, respectively. That is, the sonic Mach number is $\mathcal{M}_s \equiv V_L/c_s$, where V_L is the injection velocity, c_s is the sound velocity, and the Alfvénic Mach number is $\mathcal{M}_A \equiv V_L/V_A$, where V_A is the Alfvén velocity. The Sonic Mach number provides important clues on the role of fluid compressibility while the Alfvénic Mach number gives insight into the influence of the magnetic field in the evolution of ISM turbulence. Throughout the paper we will use the terms "compressibility" and Sonic Mach number interchangeably.

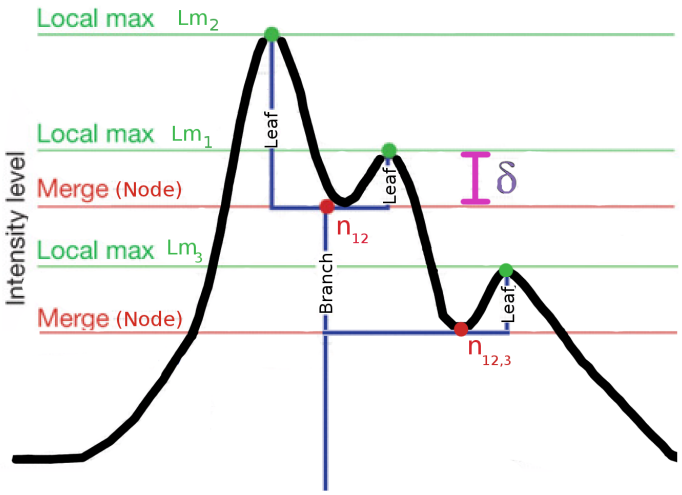

Fig. 1.— The dendrogram for a hypothetical 1D emission profile showing three local maximum (leaves) and merger points (nodes). The Dendrogram is shown in blue and can be altered by changing the threshold level δ to higher or lower values. In this example, increasing the value of δ will merge the smallest leaf into the larger structure. The local maximum (green dots) and merger points (i.e. nodes, red dot) are the values used to create a distribution ξ.

The paper is organized as follows. In § 2 we describe the dendrogram algorithm, in § 3 we discuss the simulations and provide a description of the MHD models. We investigate the physical mechanisms that create hierarchical structure in the dendrogram tree and as well as characterize the tree diagrams via statistical moments in § 4. In § 5 we compare the dendrograms of PPP and PPV. In § 6 we discuss application and investigate issues of resolution. Finally, in § 7 we discuss our results followed by the conclusions in § 8.

2. Dendrogram Algorithm

The dendrogram is a tree diagram that can be used in 1D, 2D or 3D spaces to characterize how and where local maxima merge as a function of a threshold parameter. Although this paper uses the dendrogram in 3D PPV space to characterize the merger of local maxima of emission, it is more intuitive to understand the 1D and 2D applications. A 1D example of the dendrogram algorithm for an emission profile is shown in Figure 1. In this case, the threshold value is called δ, and is the minimum amplitude above a merger point that a local

maximum must be before it is considered distinct. That is, if a merger point (or node) is given by n and a local maximum is given by Lm then in order for a given local max Lm_1 to be considered significant, $Lm_1 - n_{1,2} > \delta$. If $Lm_1 - n_{1,2} \leq \delta$. then Lm_1 would merge into Lm_2 and no longer be considered distinct.

Run	$M_s \approx$	$M_A \approx$	Sonic Nature	Magnetic Nature	Size	Comments
1	0.5	0.7	sub-sonic	sub-Alfvénic	512x512x512	
2	0.7	0.7				
3	2	0.7	super-sonic			
4	3	0.7				
5	4.4	0.7				
6	7	0.7				
7	8.4	0.7				
8	10	0.7				
9	0.5	2	sub-sonic	super-Alfvénic		
10	0.7	2				
11	2	2	super-sonic			
12	3	2				
13	4.4	2				
14	7	2				
15	8.4	2				
16	10	2				
17	2	2				
18	2	0.7		sub-Alfvénic	256x256x256	
19	2	2		super-Alfvénic		self-gravityx4
20	2	2				self-gravityx1

Fig. 2.— List of the simulations and their properties. We use different colors to differentiate the parameter space. We define the subsonic regimes as anything less then $\mathcal{M}_s$=1 and the supersonic regime as $\mathcal{M}_s > 1$. Two Alfvénic regimes exist for each sonic Mach number: super-Alfvénic and sub-Alfvénic.

For 2D data, a common analogy (see Houlahan & Scalo 1992, Rosolowsky et al. 2008) is to think of the dendrogram technique as a descriptor of an underwater mountain chain. As the water level is lowered, first one would see the peaks of the mountain, then mountain valleys (saddle points) and as more water is drained, the peaks may merge together into larger objects. The dendrogram stores information about the peaks and merger levels of the mountain chain.

The dendrogram is similar to many other statistics that employ a user defined threshold value in order to classify structure. By varying the threshold parameter δ (see Figure 1), different dendrogram local max distributions are created. An example of another statistic that utilizes a density/emission threshold value is the Genus statistic, which has proven useful for studying ISM topology (Lazarian, Pogosyan & Esquivel 2002; Lazarian 2004; Kim & Park 2007; Kowal et al. 2007; Chepurnov et al. 2008). For the Genus technique, the

variation of the threshold value is a critical point in understanding the topology of the data in question.

For our purposes, we examine the dendrogram in 3D PPV space (see Rosolowsky et al. 2008; Goodman et al. 2009 for more information on the dendrogram algorithm applied in PPV). In the 3D case, it is useful to think of each point in the dendrogram as representing a 3D contour (isosurface) in the data cube at a given level. As δ sets the definition for "local maximum," setting it too high will produce a dendrogram that may miss important substructures while setting it very low may produce a dendrogram that is dominated by noise. While δ sets the value for the minimum leaf length, the branches of the tree do not directly depend on δ, and only depend on at what intensity level a set of local maximum are joined at.

The issues of noise and the dendrogram were discussed extensively in Rosolowsky et al. 2008. While the dendrogram is designed to present only the essential features of the data, noise will mask the low-amplitude or high spatial frequency variation in the emission structures. In extreme cases where the threshold value is not set high enough or the signal-to-noise is very low, noise can result in local maxima that do not correspond to real structure. As a result, the algorithm has a built in noise suppression criteria which only recognizes structures that have 4 σ_{rms} significance above δ. Such a criterion has been previously used in data cube analysis as noise fluctuations will typically produce 1 σ_{rms} variations (Brunt et al. 2003; Rosolowsky & Blitz 2005; Rosolowsky et al. 2008).

Once the dendrogram is created, there are multiple ways of viewing the information it provides such as:

- A tree diagram (the dendrogram itself).
- 3D viewing of the isocontours and their connectivity in PPV space.
- A histogram of the dendrogram leaf and node values (i.e. intensities), which can then be further statistically analyzed.

We note that this third point is a novel interpretation of the dendrogram that we develop in this work. Here the histogram will be composed of intensity values important to the hierarchical structure of the image. This includes the leaves, denoted by Lm, and nodes, denoted with n. In this case we define a distribution:

$$\xi = \begin{pmatrix} Lm_1 & Lm_2 & Lm_3 & Lm_4 .... Lm_n \\ n_{1,2} & n_{3,4} & n_{(1,2),(3,4)} & ...n_{m,n} \end{pmatrix}$$

This interpretation is visualized in Figure 3 and further described below. To produce the dendrogram, we first identify a population of local maxima as the points which are larger than all surrounding voxels touching along the face (not along edges or corners). This large set of local maxima is then reduced by examining each maximum and searching for the smallest contour level that contains only that maximum. If this contour level is less than δ below the local maximum, that local maximum is removed from consideration in the leaf population (this difference in data values is the vertical length of the "leaves" of the dendrogram).

Once the leaves (local maxima) of the dendrogram are established, we contour the data with a large number of levels (500 specifically, see Rosolowsky et al. 2008; Goodman et al. 2009). The dendrogram "branches" are graphically constructed by connecting the various sets of maxima at the contour levels where they are joined (see Figure 1 for a 1D example). For graphical presentation, the leaves of the structure tree are shuffled until the branches do not cross when plotting. As a result, the x-axis of the dendrogram contains no information. More information on the dendrogram algorithm can be found in Goodman et al. (2009) in the Supplementary Methods section and in Rosolowsky et al. (2008).

The purpose of this paper is to use dendrogram to characterize the observed hierarchy seen in the data. We are not necessarily interested in individual clumps found in the synthetic PPV data, but rather characterizing how the structures and hierarchy found in simulations of MHD turbulence depend on parameters such as the level of turbulence, magnetic fields, and self-gravity. While turbulence has often been cited as the cause of the observed hierarchical structure in the ISM (Stutzki 1998), it is unclear to what extent magnetic fields, gas pressure, and gravity play roles in the creation of ISM hierarchy even though these parameters are known to drastically change the PDF and spectrum of both column density and PPV data (see Falgarone 1994; Kowal et al. 2007; Tofflemire et al. 2011).

3. Data

We generate a database of twenty 3D numerical simulations of isothermal compressible (MHD) turbulence by using the MHD code of Cho & Lazarian 2003 and vary the input values for the sonic and Alfvénic Mach number. We briefly outline the major points of the numerical setup.

The code is a second-order-accurate hybrid essentially non-oscillatory (ENO) scheme which solves the ideal MHD equations in a periodic box:

$$\frac{\partial \rho}{\partial t} + \nabla \cdot (\rho \mathbf{v}) = 0, \tag{1}$$

$$\frac{\partial \rho \mathbf{v}}{\partial t} + \nabla \cdot \left[\rho \mathbf{v}\mathbf{v} + \left(p + \frac{B^2}{8\pi} \right) \mathbf{I} - \frac{1}{4\pi} \mathbf{B}\mathbf{B} \right] = \mathbf{f}, \tag{2}$$

$$\frac{\partial \mathbf{B}}{\partial t} - \nabla \times (\mathbf{v} \times \mathbf{B}) = 0, \tag{3}$$

with zero-divergence condition $\nabla \cdot \mathbf{B} = 0$, and an isothermal equation of state $p = C_s^2 \rho$, where p is the gas pressure. On the right-hand side, the source term $\mathbf{f}$ is a random large-scale driving force. We drive turbulence solenoidally[2] with energy injected on the large scales. The time t is in units of the large eddy turnover time ($\sim L/\delta V$) and the length in units of L, the scale of energy injection. The magnetic field consists of the uniform background field and a fluctuating field: $\mathbf{B} = \mathbf{B}_{\rm ext} + \mathbf{b}$. Initially $\mathbf{b} = 0$. We stress that simulations are scale free and all units are related to the turnover time and energy injection scale.

We divide our models into two groups corresponding to sub-Alfvénic and super-Alfvénic turbulence. For each group we computed several models with different values of gas pressure (see Figure 2) falling into regimes of sub-sonic and supersonic. We ran 14 compressible MHD turbulent models, with 512^3 resolution, and 4 at 256^3 with 2 of these having self-gravity. We solve for the gravitation potential using a Fourier method similar to that described in Ostriker et al. 1999. The models are listed and described in Figure 2.

We use density and velocity perpendicular to the mean magnetic field in order to create fully optically thin synthetic PPV data cubes, although we also investigate dendrogram for other LOS orientations. The PPP and synthetic PPV cubes are all normalized by the mean value, i.e. $PPV_{final} = PPV_{orignial} / < PPV_{orignial} >$) Varying the optical depth will be done in a later work. We create cubes with a given velocity resolution of 0.07, which is ten times smaller then the rms velocity of the simulation ($v_{rms} = 0.7$). For reference, the sound speed of the simulations varies from $c_s = 1.4 - 0.07$ for our most subsonic to most supersonic simulations. PPV cubes are created by reorganizing density cubes into channel bins based on given velocity intervals. Additional discussion on comparing the simulations to observations is found in Section 6.

[2]The differences between solenoidal and compressive driving is discussed more in Federrath et al. 2008. One can expect driving in the ISM to be a combination of solenoidal and compressive, however both types of driving will produce shocks on a range of scales, which is what we study here.

4. Characterizing Hierarchy and Structures Created by Turbulence

We applied the dendrogram algorithm on synthetic PPV cubes with various sonic and Alfvénic Mach numbers. An example of how the the tree diagram output changes with threshold value δ is shown in Figure 3. The top row of Figure 3 shows the isosurfaces with the colors relating back to the colors in the corresponding dendrogram shown in the middle row. As the threshold intensity value δ (which, shown here with a black line, sets the definition of the local maximum or 'leaves of the tree') increases, structures in the dendrogram begin to merge with each other. The leaf and branch length and number of structures provides information on the hierarchical nature of the PPV cube. The branches are sorted to not cross, which leaves the x-axis with no information. The bottom row of Figure 3 shows the histograms of the dendrogram distribution of intensities (leaves and nodes). The red line is a reference line at intensity level 25. This distribution also changes with changing threshold value, as leaves merge with one another and the hierarchy changes.

In the next subsections, we investigate the effects of the compressibility, magnetization, and level of self-gravity on the number of structures, amount of hierarchical structure, and moments of the dendrogram distribution. We define a hierarchical dendrogram as one which has many segments on its paths and hence many levels above the root.

4.1. Sonic and Alfvenic Mach Numbers

4.1.1. Leaf and Branch Counting

We computed the dendrogram for all synthetic non-self gravitating PPV cubes with varying threshold values.

Figure 4 top shows how the total number of structures (i.e., dominant emission contours including dendrogram "leaves and branches") changes as we change δ. We plot the total number of structures vs. δ on a logarithmic scale (i.e. Log N vs Log δ) for simulations with three differing values of sonic Mach number ($\mathcal{M}_s$=8.0, 3.0, 0.7) and two values of Alfvénic Mach number. The left panel shows sub-Alfvénic models and the right shows super-Alfvénic models. Error bars are created by taking the standard deviation between different time snapshots. We note that power law tails can be seen at values of δ past the mean value (i.e. past log $\delta = 0$). We over plot the values of the slopes with solid black lines for reference.

When δ is at or slightly below the mean value of the data cubes, there is little difference in number of structures seen in the dendrogram between simulations of different sonic Mach number. This is surprising, since the structures seen in subsonic turbulence are very different

from supersonic case. In the regime where δ is at the mean value, we are sampling most of the PPV cube emission and therefore are not sensitive to the differences seen at larger threshold values which will merge low intensity structures. Once we increase δ beyond the mean however, the number of structures between the subsonic (black plus signs) and supersonic simulations (red stars and green diamonds) rapidly diverges as the emission contours due to shocks begin to stand out, and the low intensity contours merge. Because shocks create higher intensity values in the PPV cubes, the slopes in the subsonic cases are much steeper as the number of structures the dendrogram considers significant at a given threshold value rapidly falls off to zero. Subsonic models have fewer significant emission contours since they do not have density enhancements created by shocks and therefore the density/velocity contrast between subsonic and supersonic turbulence becomes clear at higher threshold values. The higher the Mach number, the more small scale enhancements we expect to see.

As δ increases, differences between supersonic ($\mathcal{M}_s$= 3.0) and very supersonic ($\mathcal{M}_s$= 8.0) cases become more apparent, as the slopes for the $\mathcal{M}_s$= 3.0 case are steeper. This is because interacting shocks in the $\mathcal{M}_s$= 8.0 are much stronger, and hence there is more contrast in the emission contours. Thus, as we increase δ, the structures merge more rapidly for lower values of the sonic Mach number.

Comparison between the left and right panels shows that the magnetic field also affects the number of structures and the trend with the threshold value. When δ is low (i.e. there is more structure in the tree) the low magnetized case (super-Alfvénic, right panel) shows slightly more structures then the highly magnetized case. However, as the threshold value increases, the number of structures decreases more rapidly in the case of the super-Alfvénic case, which is evident in that the slopes are steeper regardless of the sonic Mach number. These trends with magnetic field are due to differences between MHD and hydrodynamic turbulence. For super-Alfvénic gas (which is close to hydrodynamic), turbulent eddies can evolve with a full 3D range of motion and have more degrees of freedom then plasma turbulence in the presence of a strong magnetic field. For turbulence in the sub-Alfvénic regime, the strong field creates anisotropy in the eddies, which are stretched along the direction of the mean field line. This limits the range of motion of the eddies which in turn, limits their ability to interact. Structures in the supersonic sub-Alfvénic cases show more contrast in PPV, meaning that the local maximum are generally higher and differences from the mean are more pronounced (this will be discussed more in the next subsection with the moments). Hence, as we increase δ, the structures in sub-Alfvénic turbulence do not merge with each other as quickly as in the case of the super-Alfvénic turbulence, which has less contrast in its emission cubes.

In light of this, we might also expect the structures in sub-Alfvénic turbulence to show

less hierarchical structure overall. A test of hierarchy is to count the number of segments along the largest branch, from leaf to root. The bottom plot of Figure 4 shows the number of segments from root to leaf on the largest branch vs. the threshold parameter δ. Similar to what was shown in the top figure, the sonic Mach number has a strong relation to the amount of hierarchical structure created in the gas. Higher sonic Mach number yields more shocks which in turn produce more high density clumps and more hierarchical structures in PPV space. However, as expected from the top plot, the magnetic field seems to also play a strong role in the hierarchical branching. Comparison between the y-axis values of the left and right plots reveals that a larger Alfvénic Mach number creates more hierarchical structure in the PPV dendrogram. In the case of super-Alfvenic turbulence, magnetization is low and hence the structures created are closer to that of hydrodynamic turbulence, which is well known to show fractal behavior and hierarchical eddies. As turbulence transitions to sub-Alfvenic, it become magnetically dominated with fewer degrees of freedom. The contrast in sub-Alfvénic PPV data is higher, and hence there is less hierarchical structure as compared with super-Alfvénic turbulence.

We illustrate these findings in Figure 5. Case A shows a cloud with a global Alfvénic Mach number ≥ 1 while cases B and C show the same cloud with global Alfvénic Mach number ≤ 1 but with compression parallel and perpendicular to the field. All cases are assumed to have the same supersonic value of the sonic Mach number. Case A shows hierarchical structure forming in clumps that are not affected strongly by the magnetic field. The clumping and hierarchy is due to compression via shocks and the shredding effect of hydrodynamic turbulence. For case B and C, we now consider how this picture changes if we introduce a strong magnetic field. For shock compression parallel to the field lines (Case B), the clumps will be confined in the direction perpendicular to the field, and thus the compression will squeeze the clumps, decrease the hierarchy in the gas, create additional large density contrast. For shock compression perpendicular to the field lines, in this case the magnetic pressure relative to the shock compression is much higher, and the clumps will not feel as much of the compression. Thus in case B and C, the contrast is higher while hierarchical structure is less.

These results have interesting implications for hierarchical structures in interstellar and star forming clouds, which we will discuss more in the discussion section (section 7).

The plots in Figure 4 are for PPV cubes with LOS taken perpendicular to the mean magnetic field. We tested our results for LOS taken parallel to the mean magnetic field and found similar results.

4.1.2. Statistics of the Dendrogram Distribution

A dendrogram is a useful representation of PPV data in part because there are multiple ways of exploring the information on the data hierarchy. In this section we investigate how the statistical moments of the distribution of the dendrogram tree (see bottom panels of Figure 3 for example) changes as we change the threshold parameter δ and how these changes depend on the compressibility and magnetization of turbulence. We consider a distribution ξ containing all leaves and merging contour values in a given dendrogram. The question that forms the basis of our investigation in this section is: Do the moments of the distribution ξ have any dependencies on the conditions of the gas (i.e. the sonic and Alfvénic Mach number) and how does this relate back to the previous subsection?

The 1st and 2nd order statistical moments (mean and variance) used here are defined as follows: $\mu_\xi = \frac{1}{N}\sum_{i=1}^{N}(\xi_i)$ and $\nu_\xi = \frac{1}{N-1}\sum_{i=1}^{N}\left(\xi_i - \overline{\xi}\right)^2$, respectively. The standard deviation is related to the variance as: $\sigma_\xi^2 = \nu_\xi$. The 3rd and 4th order moments (skewness and kurtosis) are defined as:

$$\gamma_\xi = \frac{1}{N}\sum_{i=1}^{N}\left(\frac{\xi_i - \mu_\xi}{\sigma_\xi}\right)^3 \tag{4}$$

$$\beta_\xi = \frac{1}{N}\sum_{i=1}^{N}\left(\frac{\xi_i - \mu_\xi}{\sigma_\xi}\right)^4 - 3 \tag{5}$$

We calculate the moments of the dendrogram tree distribution while varying our simulation parameter space. In particular, we vary the sonic Mach number, the Alvénic Mach number, and the threshold value. We find the moments vs. the threshold parameter δ to show linear behavior. As δ increases, the number of the intermediate intensity values that make up the branches and the hierarchical nesting (i.e. the intensity values between the high intensity local maximum and the low intensity values near the trunk) merge with each other. This effect can be seen visually in Figure 3. Thus, as δ increases, the mean and variance of the distribution (example show in the bottom of Figure 3) will increase.

We plot the moments vs. $\mathcal{M}_s$ with $\delta = 4$ in Figure 6. This figure shows the full range of our simulations with sub- and super-Alfvénic combinations. Generally as the sonic Mach number increases so do the moments. We found this trend to be consistent over a range of δ values, and hence only plot one case here. Error bars, created by taking the standard deviation of the value between different time snapshots of the simulation, generally increase with sonic number as the fluctuations become increasingly stochastic and shock dominated. Physically, the increase of the moments of ξ is related to the compressibility of the model and

more supersonic cases display more prominent clumpy features, which drive up the both the average and the variation from average. The tails and peak of the distribution also become increasingly skewed and kurtotic towards higher values of intensity and the distribution becomes more peaked around the mean value.

It is interesting to note that a strong dependency on the magnetization of the model exists, particularly as the sonic number goes up. The sub-Alfvénic simulations show increased moments, which implies that they exhibit more contrast (mean value is higher) and more skewed/kurtotic distributions in their gas densities. This result is to be expected based on the findings of the previous subsection, which showed sub-Alfvénic turbulence to exhibit less hierarchical nesting.

In the above analysis the distribution ξ included all leaves and branches of the dendrogram tree. We could further cut the tree into its respective branches and leaves and analyze the distributions separately, which provides additional constraints on the parameters. We investigated the statistical moments on the histograms of the branch lengths, leaf lengths, and leaf intensities and found the trends discussed above to be consistent with the results of Figure 6, and hence do not include the plots.

4.2. Self-Gravity

4.2.1. Leaf and Branch Counting

The issues of the importance of self-gravity in simulations have been raised by a number of authors (Padoan et al. 2001; Li et al. 2004; Goodman et al. 2009; Federrath et al. 2010). While self-gravity is known to be of great importance to accretion disk physics and protostellar collapse, its role in diffuse gasses is less obvious. As the dendrogram provides insight into the hierarchical structure of the PPV space, it can potentially be used to explore whether gravity has a major effect on both the structure of the hierarchy and the distribution of dominant emission contours.

Figure 7 shows the tree diagrams at constant δ=45 for super-Alfvénic supersonic simulations with different levels of self-gravity. This large value of δ is used in order to not over crowd the dendrogram with branches. We choose a super-Alfvénic model because super-Alfvénic supersonic turbulence is thought by many to be the type of conditions that exist in star forming molecular clouds (see Padoan & Nordlund 1999). In this figure, high gravity is ≈ 4 orders of magnitude larger then the weak gravity case. Gravity affects the dendrogram both in terms of structure and number of significant emission regions. Visually from Figure 7, one can see at constant δ, higher gravitational strength creates a dendrogram that has

more hierarchical structures. We use a high value of δ to keep the plots from being over crowded with branches.

We show the number of structures vs. δ in Figure 8 using a logarithmic scale similar to the top of Figure 4. Our analysis spans the ranges of δ from 4-40. High and low levels of self-gravity with Alfvén number=2.0 and sonic number=7.0 and the corresponding no self gravity case are plotted in black, red, and blue, respectively. It is clear that the case with no self-gravity (symbolized with blue diamonds) shows less overall structure compared with the cases with self-gravity. High gravity simulations have significantly more nested structures and more contours considered to be areas of significant emission then low gravity. Interestingly, the power law behavior that is seen in the case with no gravity in Figure 8 and all of the cases in Figure 4 is absent for simulations with gravity. The absence of power-law behavior in the number of structures vs. δ may be used in ISM clouds to determine if self-gravity is important for cloud dynamics

4.2.2. Statistics of the Dendrogram Distribution

We show how self-gravity affects the dendrogram distribution as we vary δ in Figure 9 for a simulations with Alfvén number=2.0 and Sonic number=7.0. Higher levels of self-gravity show increases in all four moments over a range δ. The trends are smooth and linear as δ varies. The moments for this simulation with self-gravity are similar in magnitude to the case without self-gravity in the $\delta = 4$ example shown in Figure 6.

5. Dendrograms of PPP vs. PPV

The issue of interpreting structures seen in PPV space has vexed researchers for over a decade (see Pichardo et al. 2000). How the structures in PPV translate to PPP depends on many factors, most importantly the nature of the turbulent environment. The dendrogram presents a unique way of studying how the hierarchy of structures seen in density space (PPP) relate to PPV space via simulations. From analyzing the spectrum of density and velocity with techniques such as VCS, one finds that the spectrum of PPV is dominated by density in the case of supersonic turbulence while in the case of subsonic turbulence, velocity dominates. One might expect these signatures to also show up in a dendrogram analysis. This is useful for observers especially, since it is critical that they be able to interpret the morphologies observed in PPV space in a physically meaningful way.

For turbulent clouds, it is never the case that the structures in PPV have a one-to-one

correspondence with the density PPP, although this assumption may be more appropriate for some environments then others. We show a simple example illustrating this in Figure 10 which shows synthetic PPV data cubes (left), and a PPP data cube (i.e. a density cube, right) for subsonic super-Alfvénic turbulence. The bottom left PPV cube has constant density/column density, while the top left PPV cube's corresponding density cube is shown on the right.

Interestingly, the bottom left PPV cube has a very similar level of structure to it as compared with the top PPV cube, despite the fact that the column density of the bottom cube is constant. This points out the well known fact that there is not a one-to-one correspondence with PPV and PPP space. In fact, in this example (a subsonic model) most of the structures are due to the velocity rather then the density. Figure 10 illustrates the dominance of velocity in the subsonic case in the bottom PPV cube. Fluctuations in PPV here are *entirely driven by the turbulent velocity field*.

To illuminate this point further Figure 11 shows PPP and PPV dendrograms for supersonic turbulence with $\mathcal{M}_s$=8.0 (middle) and subsonic turbulence with $\mathcal{M}_s$=0.5 (bottom). We also show the corresponding isosurfaces for the supersonic case in the top row. Comparing PPV and PPP should be done with care as they are different spaces. Here we increased the value of δ until the PPP dendrogram becomes mostly leaves, that is, they have little hierarchy. The leaves are reached at $\approx \delta = 40$. We took the corresponding optically thin PPV cube and applied the dendrogram with the same $\delta = 40$ threshold value. If the dominate emission is due to *density* then the leaves should be similar for both PPV and PPP. All PPV and PPP cubes have mean value of unity.

Interestingly, the supersonic turbulence dendrogram for density looks very similar to the corresponding PPV dendrogram for the same δ at the level of the leaves. For the subsonic case we see that the dendrogram of density and PPV look nothing alike (same δ). In this case, the velocity field dominates PPV space. Hence, we don't show the isosurfaces for the subsonic case. In supersonic turbulence, the highest density peaks correspond to the highest intensity fluctuation in the PPV. This implies that if one knows the turbulence in question is supersonic, the structures in PPV space at the level of the leaves can be generally interpreted as 3D density structures. However, if the turbulence is subsonic in nature, this assumption may not be appropriate.

6. Application

The different parts of the dendrogram tree show dependencies on parameters of turbulence that are particularly important to both studies of star forming regions and the diffuse ISM. When analyzing a particular data set, one should keep in mind that comparisons between the observational and scaled numerical data, or comparisons between different clouds or objects in the data are the most useful means of extracting these parameters.

Our simulations can be scaled to observations by specifying physical size of the simulation volume, the isothermal sound speed of the gas, and mass density. For example, the velocity scale factor v_0,which relates simulation velocities to physical velocities, is given by:

$$v_0 = Cs_{obs}/Cs_{sim} = cs_{obs}\sqrt{\rho_{sim}/P_{sim}} \tag{6}$$

where Cs is the sound speed, P is the gas pressure, and ρ is the density. More information on scaling simulations to observations can be found in Hill et al. 2008

We include the effects of changing the velocity resolution, thermal broadening, and smoothing in the next subsection.

6.1. Smoothing

We investigate how smoothing and data resolution affect the dendrogram. When dealing with observational data one must always consider the effect that the telescope beam smoothing will have on the measurement. The observations are rarely done with pencil beams and the measured statistics change as the data is averaged. We expect the effect of smoothing to depend on a dimensionless number, namely, the ratio of the size of the turbulence injection scale to the smoothing scale.

We apply the same technique that was applied in the previous sections, i.e. exploring number of structures and moments of dendrogram tree statistics, however now we include a boxcar smoothing kernel (truncating the edges). We expect that smoothing will affect supersonic turbulence and cases of high self-gravity the most. In this case, shocks and small scale gravitational clumps become smoothed out and more difficult for the algorithm to identify. In the subsonic or low gravity cases, smoothing makes less of a difference since the gas is already diffuse and less hierarchical.

We show how the moments and number of structures changes with smoothing size (in pixels) in Figure 12. One could also discuss smoothing beam size in terms of the injection scale of the turbulence. For instance, 7 pixel smoothing represents a beam scale that is 30 times smaller then our injection scale of turbulence.

We found that generally, subsonic and transonic turbulence are not as affected by smoothing compared to highly supersonic models. In light of this, we plot the moments and number of structures vs. δ for different smoothing degrees for a highly supersonic model with $\mathcal{M}_s$=8.0 in Figure 12. Two panels show different Alfvénic regimes with the y-axis the same for both for ease of comparison. Black lines indicate no smoothing, while red and blue indicate three and seven pixel smoothing, respectively. Error bars are produced by taking the standard deviation between different time snapshots of the simulations with well developed turbulence.

As smoothing increases for this supersonic model, we see that the values of the moments as well as the total number of structures decreases. However, even out to seven pixel smoothing the differences between the Aflvénic cases is evident in the mean and variance, respective of the error bars. Furthermore, the trends with the threshold parameter do not change when we introduce smoothing, which gives us further confidence that this technique can be applied to the observational data. Other than the change in amplitude, the trends remain the same as what was seen in Section 4.

6.2. Velocity Resolution

In addition to smoothing we must also consider the effects of velocity resolution. As the velocity resolution changes in PPV space, so do the structures observed. We investigated how the moments of the dendrogram branch + leaf distribution changed when we vary the velocity resolution. We find that the number of substructures drops dramatically as the velocity resolution decreases, from several hundreds to several dozen when changing the velocity resolution from $v_{res} = 0.07$ to $v_{res} = 0.7$. This effect corresponds to the channel sampling dropping from ≈ 60 down to 15 channels. This may provide too low a number of statistics in the dendrogram distribution to look at the moments, however the general trends with the physical parameters stay consistent with section 4. The same holds for the case where we increase the velocity resolution an order of magnitude (up to $v_{res} = 0.007$).

6.3. Thermal Broadening

The bulk of this paper focuses on the effects of turbulence and magnetic fields in the creation of hierarchical structure in ISM clouds, however thermal broadening effects must also be considered as well. Convolution with a thermal broadening profile (i.e. a Gaussian) will smooth out the velocity profiles and generally decrease the intensities. We convolve the

line profiles of eight of our simulations with sonic Mach numbers ranging from $\mathcal{M}_s$=2.0-10 with Gaussian profiles to mimic the effects of thermal broadening. The thermal Gaussian has FWHM given as the ratio of the turbulent line width to the sonic Mach number. As thermal broadening will change the intensity range of our simulations, we accordingly change the values of the threshold parameter δ. We scale δ down from the range used in Section 4 by a factor of $< PPV_{thermal+turbulent} > / < PPV_{turbulent} >$, in order to fully sample how the contours merge in the new cubes.

We show the effects of including thermal broadening on the number of structures and amount of hierarchical structure in Figure 13. While the threshold value had to be lowered due to the intensity change in the PPV cubes, the trends are similar to those presented in Section 4 when thermal broadening was not included. Namely, that supersonic super-Alfvénic turbulence generally shows more overall structure and more hierarchical structure. The main difference seen with the inclusion of thermal broadening is that the slopes of the power law trends of log N vs. log δ are shallower in all cases. The slopes for the sub-Alfvénic panel are -1.6, -1.2, -0.48, -0.2 for $\mathcal{M}_s$=2.0, 3.0, 8.0 and 10, respectively. The slopes for the super-Alfvénic panel are -1.8, -1.7, -0.7, -0.25 for $\mathcal{M}_s$=2.0, 3.0, 8.0 and 10, respectively. For reference the slopes for $\mathcal{M}_s$=3.0 and 8.0 from Figure 4 were -2.2 and -1.1, respectively for sub-Alfvénic turbulence and -3.3 and -1.67 for super-Alfvénic turbulence.

Similarly to Figure 4, the super-Alfvénic slopes remain steeper then the sub-Alfvénic. This shows that the effects seen in the previous sections are due primarily to the level of turbulence and the Alfvénic Mach number in the simulations, and are not masked over with thermal broadening.

7. Discussion

Hierarchical tree diagrams are finding more applications in interstellar studies, not only to locate clumps and calculate their properties, but also for characterizing properties of the physics present in interstellar and molecular gas. In this paper we used dendrograms to analyze how turbulence, magnetic fields and self-gravity shape the amount of structure and gas hierarchy in isothermal simulations. We also examined the changes in the distribution of the dendrogram as we vary the threshold parameter δ. This is analogous to changing the corresponding threshold parameter in other techniques that rely on contouring thresholds, e.g. in the Genus analysis (see Chepurnov et al. 2009). By varying δ we obtained a new outlook on the technique; in particular, we found that the dendrogram distribution and hierarchy have a strong dependency on the magnetization and compressibility of the gas and are sensitive to the amount of self-gravity.

7.1. The Hierarchical Nature of MHD Turbulence

The number of structures and the amount of hierarchy formed by MHD turbulence has interesting implications for the evolution of ISM clouds and for the star formation problem. In section 4 we found that more hierarchical structure and more overall structure was created in the presence of supersonic super-Alfvénic turbulence. We also found that the inclusion of self-gravity enhanced these trends. The relationship between the magnetization and the cloud dynamics is in the process of being understood, especially in regards to star formation. Star forming clouds are known to be hierarchical in nature and magnetized, but the exact Alfvénic nature is less clear. The results from this work seem to suggest that very hierarchical clouds might tend towards being super-Alfvénic. Several authors have suggested a variety of evidence for molecular clouds being super-Alfvénic. This includes the agreement of simulations and observations of Zeeman-splitting measurements, B vs.ρ relations, $\mathcal{M}_A$ vs. ρ relations, statistics of the extinction measurement etc. (Padoan & Nordlund 1999; Lunttila et al. 2008; Burkhart et al. 2009; Crutcher et al. 2009; Collins et al. 2012). Furthermore a study done by Burkhart et al. 2009 found that, even in the presence of globally sub-Alfvénic turbulence, the highest density regions tend towards being locally super-Alfvénic. This suggests that even in the case of globally sub-Alfvénic turbulence, the densest regions might be super-Alfvénic. It is interesting that the dendrogram technique also points to super-Alfvénic turbulence as an avenue for hierarchical structure creation. This provides motivation for the dendrogram technique to be applied to the observational data with varying threshold value δ in order to see how the nature of the hierarchical structure and total number of structures change in the observations.

7.2. Sonic and Alfvénic Mach Numbers from the Observations

In the paper above we provided a systematic study of the variations of the dendrogram δ with the sonic and magnetic Mach numbers. These numbers are critical for understanding most of processes in galactic diffuse and molecular gas, including the process of star formation. Thus, the dendrogram provides an avenue of obtaining these parameters via comparing observations and simulations and/or as a technique for investigating what processes are creating hierarchical structure in ISM gas.

We view this work as the springboard for applying the technique to the actual data. We claim that for reliable studies of the interstellar media and molecular clouds it is most advantageous to combine different techniques. For instance, applying the VCA and VCS techniques to PPV data (see Lazarian 2009 for a review), one can obtain the velocity and density spectra of turbulence. While these measures are known to depend on $\mathcal{M}_s$ and to a

lesser degree on $\mathcal{M}_A$ (see Beresnyak, Lazarian & Cho 2005, Kowal et al. 2007, Burkhart et al. 2009), the utility of the spectra is not in measuring these quantities. Spectra provide a unique way to investigate how the energy cascades between different scales, and shows whether comparing observations with the simulations with a single scale of injection is reasonable.

The analysis of the anisotropies of correlations using velocity centroids provides an insight into media magnetization, i.e., provides $\mathcal{M}_A$ (Lazarian et al. 2002, Esquivel & Lazarian 2005), which is complimentary to the technique described in this paper. Studies of the skewness and kurtosis of the PDFs (see Kowal et al. 2007, Burkhart et al. 2009, 2010) provides measures of the sonic Mach number $\mathcal{M}_s$. Similarly, Tsallis statistics measures (Esquivel & Lazarian 2010, Tofflemire et al. 2011) provide additional ways of estimating both $\mathcal{M}_s$ and $\mathcal{M}_A$. We feel the approach to obtaining these parameters should be conducted with synergetic use of multiple tools, such as was done in Burkhart et al. 2010 on the SMC. We feel the dendrogram is a unique tool as it can classify the hierarchical nature of the data and that it should be added to a standard set of statistical-tools for studies of ISM data.

All these techniques provide independent ways of evaluating parameters of turbulence and therefore their application to the same data set provides a more reliable estimate of key parameters such as compressibility, magnetization, and degree of self-gravity. Dendrograms have some advantages over other statistics designed to search for turbulence parameters, in that one can analyze the resulting tree diagram in many different ways, as highlighted in this paper and in previous works. These include finding local maxima, calculating physical properties of dominate emission, exploring how those clumps are connected in PPV, varying the threshold and calculating moments and level of hierarchy. Of course, one should keep in mind that the medium that we investigate observationally is far from simple. Multiple energy injection sources, for example, are not excluded. Thus obtaining a similar answer with different techniques should provide us with additional confidence in our results.

Finally, we should stress, that for studies of astrophysical objects the dendrogram and other statistical measures can be applied locally to different parts of the media. For instance, Burkhart et al. (2010) did not characterize the entire SMC with one sonic Mach number. Instead, several measures were applied to parts of the SMC in order to obtain a distribution of the turbulence in the galaxy. A similar local scale selection was applied also to the SMC in Chepurnov et al. (2008) using the Genus technique. The same technique should be used to parts of the ISM in the Milky way and may be attempted for GMCs. Correlating the variations of the turbulence properties with observed properties of the media, e.g. star formation rate should provide insight into how turbulence regulates many key astrophysical processes.

8. Summary

We apply dendrograms to isothermal MHD simulations with varying levels of gravity, compressibility and magnetization. We find that the dendrogram is a promising tool for studying both gas connectivity in the ISM as well as characterizing turbulence. In particular we find that:

- We propose using statistical descriptions of dendrograms as a means to quantify the degree of hierarchy present in a PPV data cube.
- Shocks, self-gravity, and super-Alfvénic turbulence create the most hierarchical structure in PPV space.
- The number of dendrogram structures depends primarily on the sonic number and the level of self-gravity and secondarily on the global magnetization.
- The first four statistical moments of the distribution of dendrogram leaves and connecting have monotonic dependencies on the level of self-gravity and the sonic and Alfvén Mach numbers over a range of δ.
- The dendrogram provides a convenient way of comparing PPP to PPV in simulations. Density structures are dominant in supersonic PPV and not in subsonic. Thus it is more justifiable to compare PPV directly to PPP when the gas is known to be supersonic.

B.B. acknowledges support from the NSF Graduate Research Fellowship and the NASA Wisconsin Space Grant Institution. B.B. is thankful for valuable discussions and the use of the Dendrogui code via Chris Beaumont. A.L. thanks NSF AST 0808118, the Center for Magnetic Self-Organization in Astrophysical and Laboratory Plasmas for financial support. This work was completed during the stay of A.L. as Alexander-von-Humboldt-Preisträger at the Ruhr-University Bochum. A.G. acknowledges support from NSF Grant No. AST-0908159. E.R. is supported by a Discovery Grant from NSERC of Canada.

REFERENCES

Armstrong,J. W., Rickett, B. J., Spangler, S. R., 1995, ApJ, 443, 209

Ballesteros-Paredes, J., Klessen, R. S., Mac Low, M.-M., & Vazquez-Semadeni, E. 2007, in Protostars and Planets V, ed. B. Reipurth, D. Jewitt, & K. Keil (Tucson, AZ: Univ. of Arizona Press), 63

Beresnyak, A., Lazarian, A., Cho, J., 2005, ApJ, 624, 93

Berkhuijsen E., Fletcher, A., 2008, MNRAS, 390, 19

Brunt, C. M., Kerton, C. R., & Pomerleau, C., 2003, ApJS, 144, 47

Brunt, C., & Heyer, M., 2002, ApJ, 566, 27

Brunt, C., 2010, A&A, 513, 67

Burkhart, B., Falceta-Goncalves, D., Kowal, G., Lazarian, A., 2009, ApJ, 693, 250

Burkhart, B., Stanimirovic, S., Lazarian, A., Grzegorz, K., 2010, ApJ, 708, 1204

Burkhart, B., Lazarian, A., Gaensler, B., 2012, ApJ, 708, 1204

Burkhart, B., & Lazarian, A., 2011, IAUS, 274, 365

Chepurnov, A., Gordon, J., Lazarian, A., & Stanimirovic, S.,2008, ApJ, 688, 1021

Chepurnov, A., & Lazarian, A. 2009, ApJ, 693, 1074

Chepurnov & Lazarian, 2010, ApJ, 710, 853

Cho, J. & Lazarian, A. 2003, MNRAS, 345, 325

Collins et al., 2012, ApJ, 750, 13

Crutcher, R., Hakobian, N., Troland, T., 2009, ApJ, 692, 844

Elmegreen, B. G., & Elmegreen, D. M. 1983, MNRAS, 203, 31

Elmegreen, B. G., & Scalo, J. 2004, ARA&A, 42, 211

Elmegreen, B. G., 2011, Star Formation in the Local Universe, Eds. C. Charbonnel & T. Montmerle, EAS Publications Series

Esquivel, A, & Lazarian, A., 2005, ApJ, 295,479

Esquivel, A., & Lazarian, A., 2010, ApJ, 710, 125

Falgarone, E., Lis, D. C., Phillips, T. G., Pouquet, A., Porter, D. H., & Woodward, P. R. 1994, ApJ, 436, 728

Ferriere, K., 2001, RvMP, 73, 1031

Federrath, C., et al., 2008, ApJ, 688, 79

Federrath, C., et al., 2010, ApJ, 713, 269

Feitzinger, J. V., & Galinski, T. 1987, A&A, 179, 249

Frisch, U., 1995, Turbulence, Univ. of Cambridge Press

Gaensler et al., 2011, Nature, 478, 214-217

Gill, A.G., & Henriksen, R.N., 1990, ApJ, 365, L27

Goodman et al., 2009, Nature, 457, 63

Goodman, A., Pineda, J., Schnee S., 2009, ApJ, 692, 91

Haverkorn, M., & Heitsch, F., 2004, A&A,421, 1011

Hill, A. et al., 2008, ApJ, 686, 363

Houlahan P., & Scalo J., 1992, ApJ, 393, 172

Kang, H., Ryu, D., & Jones, T. W., 2009, ApJ, 695, 1273

Kainulainen, J., Beuther, H., Banerjee, R., Federrath, C., Henning, T., 2011, A&A, 530, 64

Kim, S., Park, G., 2007, ApJ, 663, 244

Kowal, G., Lazarian, A. & Beresnyak, A., 2007, ApJ, 658, 423

Larson, R.B. 1981, MNRAS, 194, 809

Lazarian, A., 2004, J. Korean Astron. Soc., 37, 563

Lazarian, A., 2009, SSR, 143, 357

Lazarian A., & Esquivel, A., 2003, ApJ, 592, 37

Lazarian, A. & Pogosyan,D., 2000, ApJ, 537, 720

Lazarian, A. & Pogosyan, D., 2004, ApJ, 616, 943

Lazarian,A. & Pogosyan,D., 2006,ApJ, 652, 1348

Lazarian, A. & Pogosyan,D., 2008,ApJ, 686, 350

Lazarian, A., Pogosyan, D., & Esquivel, A. 2002, in ASP Conf. Proc. 276, Seeing Through the Dust: The Detection of H I and the Exploration of the ISM in Galaxies, ed. A. R. Taylor, T. L. Landecker, & A. G. Willis (San Francisco: ASP), 182

Li, P. S., Normand, M., Mac Low, M., Heitsch, F., 2004, ApJ, 605, 800

McKee, C., Ostriker, E., 2007, , ARA&A, 45, 565

Ossenkopf, V., & Mac Low, M.-M., 2002, A&A, 390, 307

Ossenkopf, V., Esquivel, A., Lazarian, A., & Stutzki, J. 2006, A&A, 452, 223

Ostriker, E., Gammie, C., Stone, J., 1999, ApJ, 513, 259

Padoan, P., & Nordlund, A., 1999, ApJ, 526, 27

Padoan, P., Rosolowsky, E. W., & Goodman, A. A. 2001, ApJ, 547, 862

Padoan, P., Nordlund, A., Rognvaldsson, O. E., & Goodman, A. A., 2001, in ASP Conf. Ser. 243, From Darkness to Light: Origin and Evolution of Young Stellar Clusters, ed. T. Montmerle, & P. Andre (San Francisco: ASP), 279

Padoan, P., Goodman, A., Juvela, Mika, 2003, ApJ, 588, 881

Padoan, P., Juvela, M., Kritsuk, A. G., & Norman, M. L. 2009, ApJ, 707, L153

Pichardo et al. 2000, ApJ, 532, 353

Podani, J., Engloner, A., & Major, A., 2009, Stat. Appl. Genet. Mol. Biol., 22.

Price, Federrath, & Brunt, 2011, ApJ, 727

Rosolowsky, E., Goodman, A., Wilner, D., Williams, J.,1999, ApJ, 524, 887

Rosolowsky, E., & Blitz, L., 2005, ApJ, 623, 826

Rosolowsky, E. W., Pineda, J. E., Kauffmann, J., & Goodman, A. A. 2008, ApJ, 679, 1338

Sawlaw W. & Haque-Copilah, S., 1998, ApJ 509, 595

Spangler, S. R., & Gwinn, C. R. 1990, ApJ, 353, L29

Toffelmire, B., Burkhart, B., Lazarian, A., 2011, ApJ, 736, 60

Scalo, J.S. 1985, in Protostars and Planets II, ed. D.C Black and M. S. Matthews, (Tucson: Univ. of Arizona Press), p. 201

Scalo, J. 1990, in Physical Processes in Fragmentation and Star Formation, eds. R. Capuzzo-Dolcetta, C. Chiosi, & A. Di Fazio, Dordrecht: Kluwer, p. 151

Stutzki, J., Bensch, F., Heithausen, A., Ossenkopf, V., Zielinsky, M., 1998, A&A, 336,697

Vazquez-Semadeni, E., 1993, ApJ, 423, 681

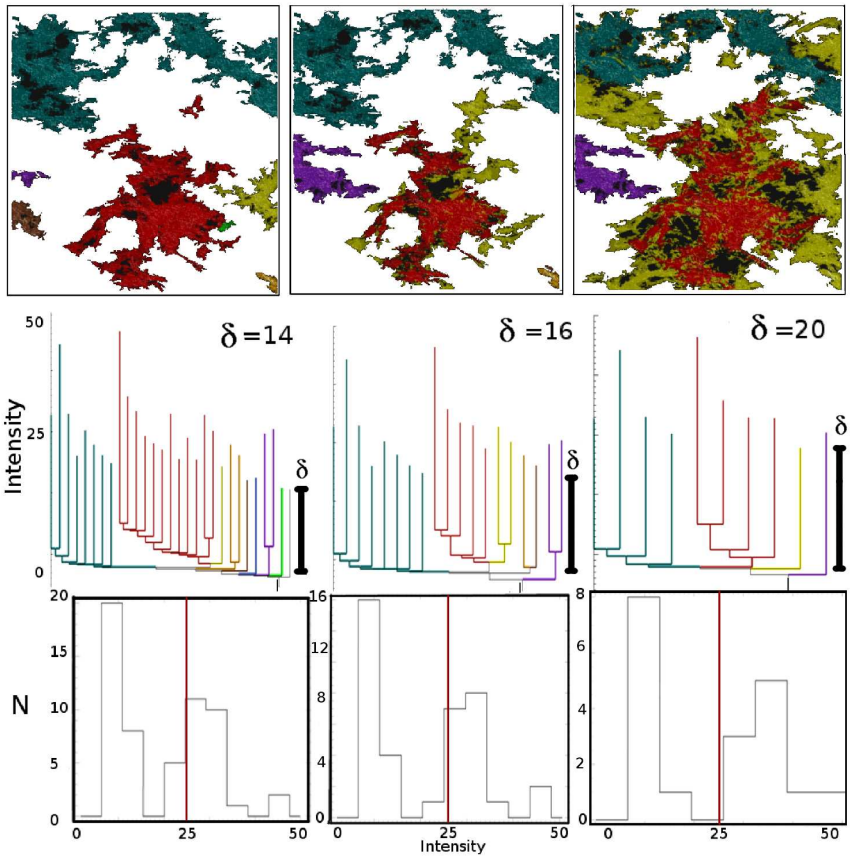

Fig. 3.— Different ways of viewing dendrogram information used in this paper. Here we show an example for supersonic sub-Alfvénic turbulence (model 3 from Figure 2) for threshold values δ=14,16,20 (left, center, right columns). The top row represents the isosurfaces in the PPV data and the middle row is the corresponding dendrogram (the black line is a reference marker for δ) with colors matching to the isosurface structures. Note there is no information on the x-axis of the tree diagram as the branches are sorted not to cross. However this still preserves all information about connectivity and hierarchy at the expense of positional information. The bottom row is the histogram of the resulting tree diagram, including the leaves, branches and nodes. The red line is a reference marker at intensity level 25. The units of intensity on the y-axis of the tree diagrams in the middle row could be in brightness temperature (T_b) for scaled simulations or observations.

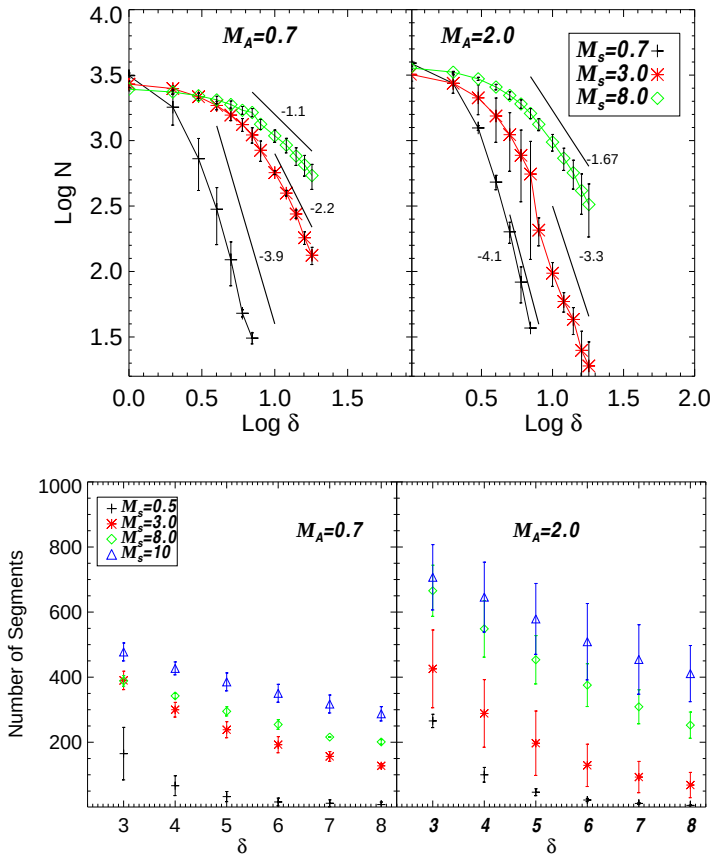

Fig. 4.— Top: Number of Structures (leaves and branches) vs. δ for six different simulations. Error bars are created by running the analysis for multiple time snapshots of the well-developed turbulence. Bottom: Number of segments from root to leaf on the largest branch of the tree vs. δ. The left panel is shows higher magnetization (sub-Alfvénic) while the right shows lower magnetization (super-Alfvénic). Both panels have the y-axis set to the same range for ease of comparison. Hierarchical structure is created both by shocks (high sonic Mach number cases) and a high Alfvénic Mach number).

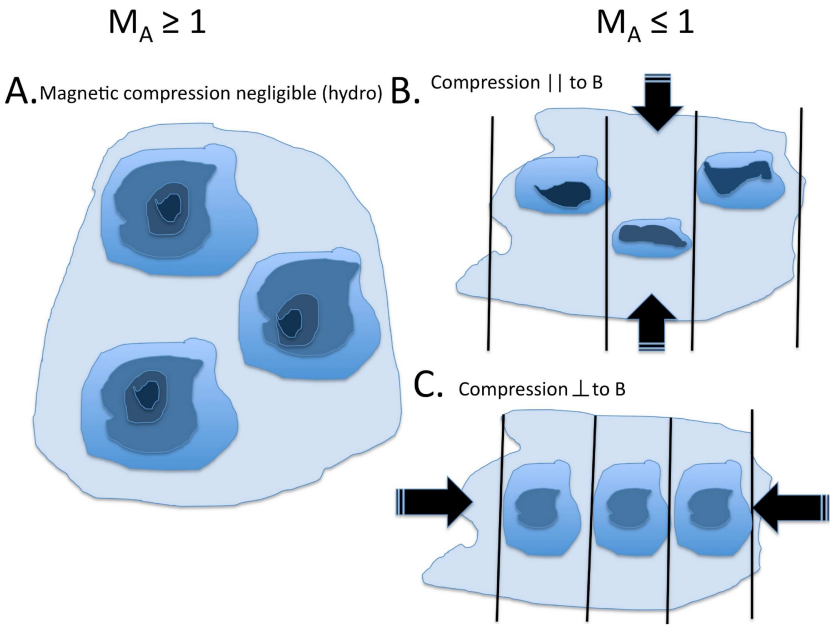

Fig. 5.— Illustration of supersonic clouds with different magnetic regimes and how this affects the observed clumps. Panel A shows a case with very low Alfvénic Mach number or a case of hydrodynamic turbulence. In this case, turbulence allows the creation of hierarchical structure with no limitation on the gas motion. Panels B and C show a cloud with higher magnetization (sub-Alfvénic) with compression parallel and perpendicular to the field lines. In the sub-Alfvenic cloud, motions will be correlated due to the strong field and the magnetic field will restrict shock compression perpendicular to the field lines (panel C). For shocks parallel to the field (panel B), increased compression will occur which will enhance contour contrast and decrease hierarchy.

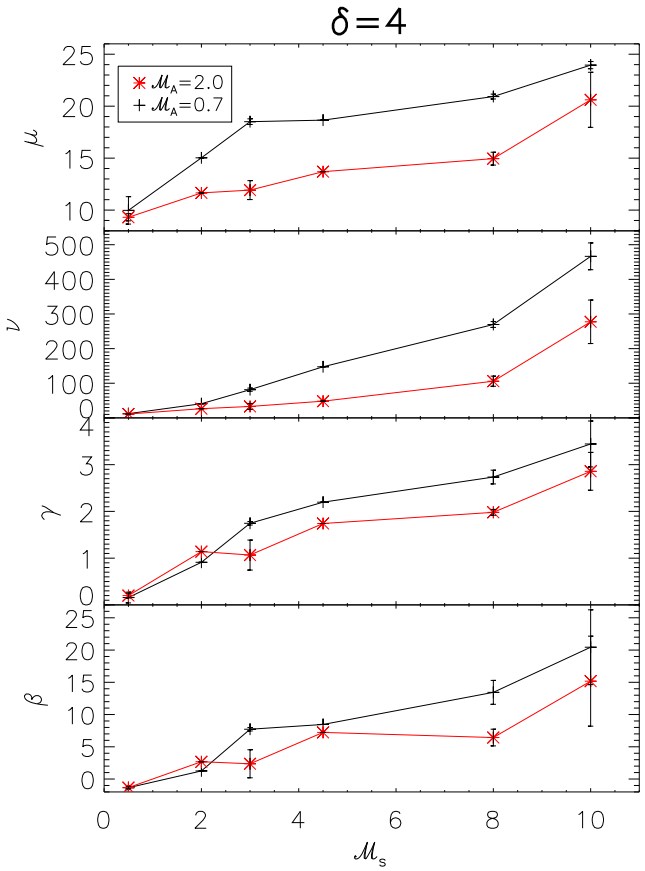

Fig. 6.— Moments of the dendrogram tree (leaves + branches) vs. $\mathcal{M}_s$ for twelve different simulations spanning a range of sonic numbers from 0.5 to 10. Here we have chosen δ=4. Panels show mean, variance, skewness and kurtosis of the distribution. Sub-Alfvénic is shown in black color and super-Alfvénic in red color.

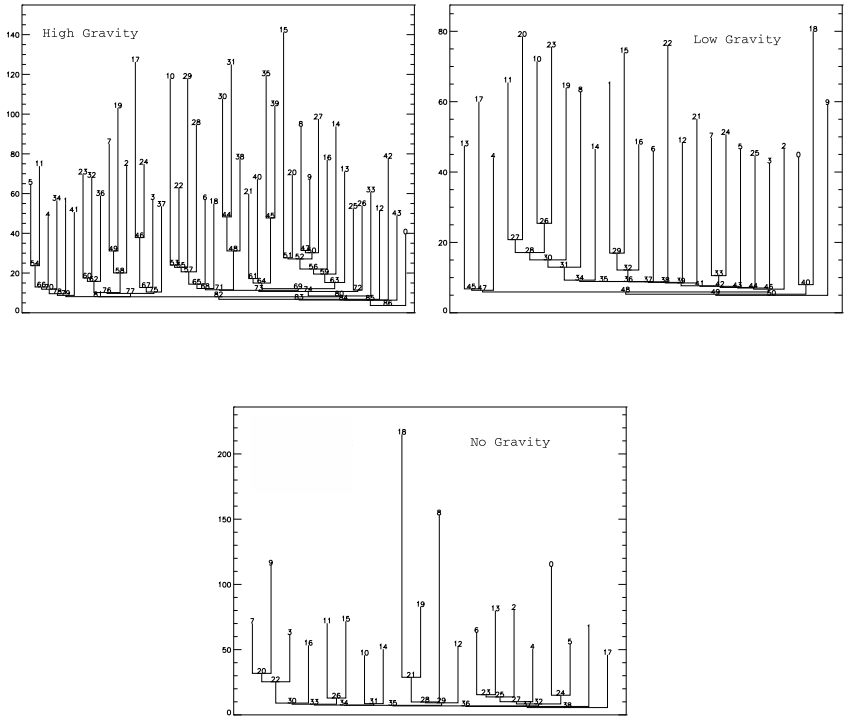

Fig. 7.— Effects of self-gravity on a 256^3 ideal MHD simulation with Alfvén number=2.0 and sonic number=7.0 with $\delta = 45$. A high value of δ is used to keep the plots from being over crowded with branches. The high self-gravity simulation is on the left, lower self-gravity in the center, and no gravity on the far right.

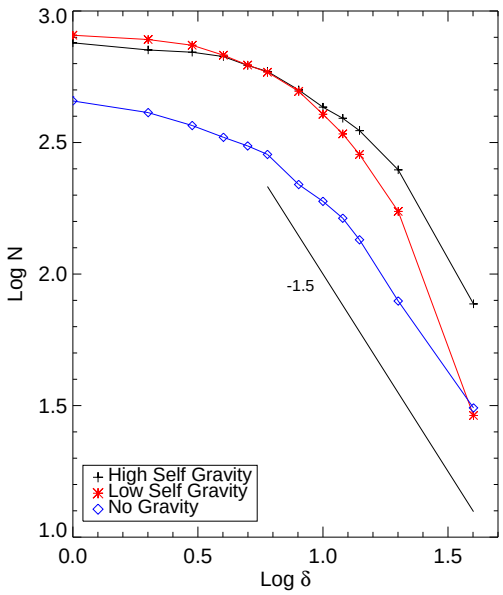

Fig. 8.— Total number of structures (branches and leaves) vs. δ on a log-log scale. Black plus signs indicated high gravity ≈ 4 orders of magnitude higher then the low gravity cases shown with red stars. Both of these have Alfvén number=2.0 and Sonic number=7.0. Comparison with a non self-gravitating simulation with Alfvén number=2.0 and sonic number=7.0 is shown with blue diamonds. We include a solid black line with slope=-1.5 to show the power-law nature of the non self-gravitating case.

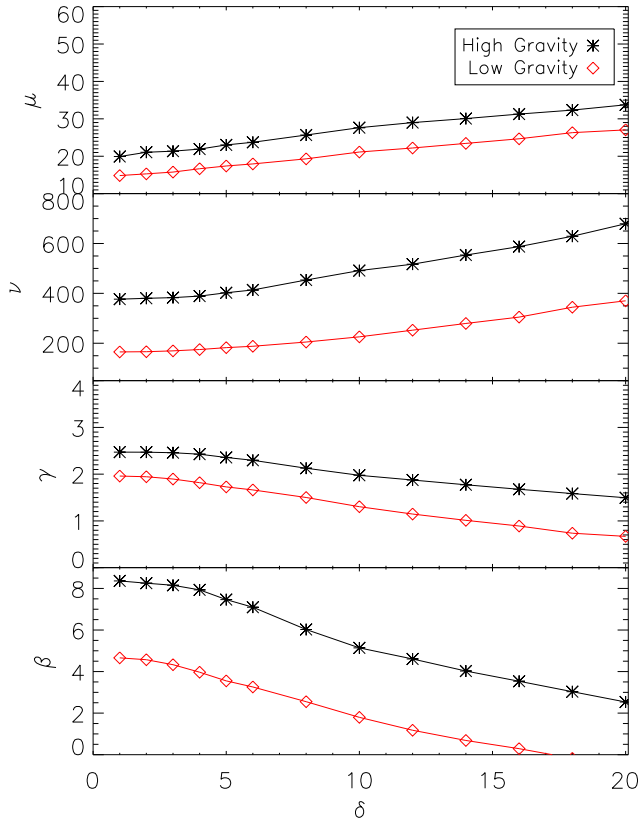

Fig. 9.— Moments of the dendrogram distribution vs. δ for models with self-gravity. High self-gravity (black lines) is 4x stronger then low self-gravity (red lines). Higher self-gravity shows increased amplitudes in the dendrogram (reflected in the mean), higher variance in values, and more skewed and peaked distributions, which are reflected in the skewness and kurtosis.

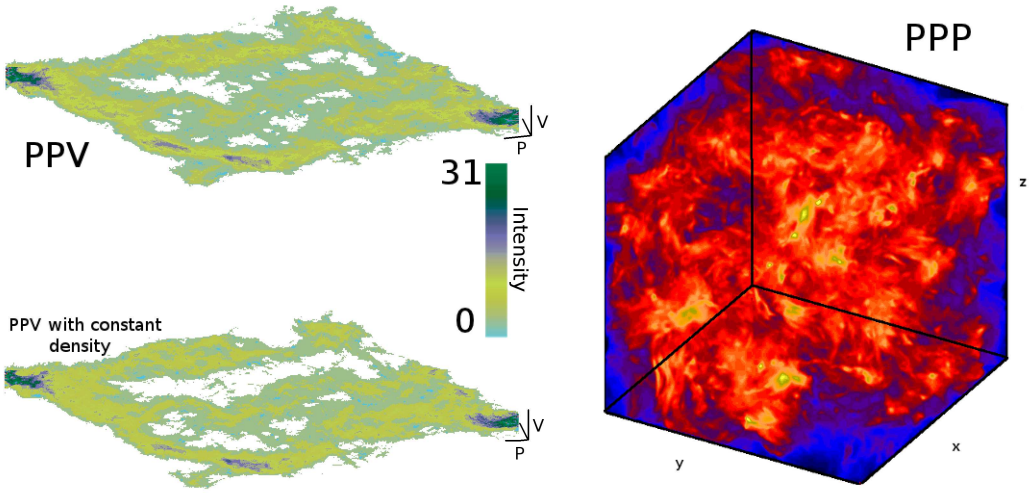

Fig. 10.— Example of a synthetic PPV data cubes with vertical axis being the velocity axis (left), and PPP data cube (right) for subsonic super-Alfvénic turbulence. Integrating along the velocity axis of PPV restores the column density map which can also be obtained from the 3D density cube. The bottom left PPV has PPP density equal to unity, and hence a constant column density. Structure in this PPV cube is due to *pure velocity fluctuations*, yet it still shows structure. This figure highlights the need to be cautious when translating the structures seen in PPV to PPP. The quantitative relation between the fluctuations in PPV and underlying density and velocity fluctuations is provided in Lazarian & Pogosyan (2000)

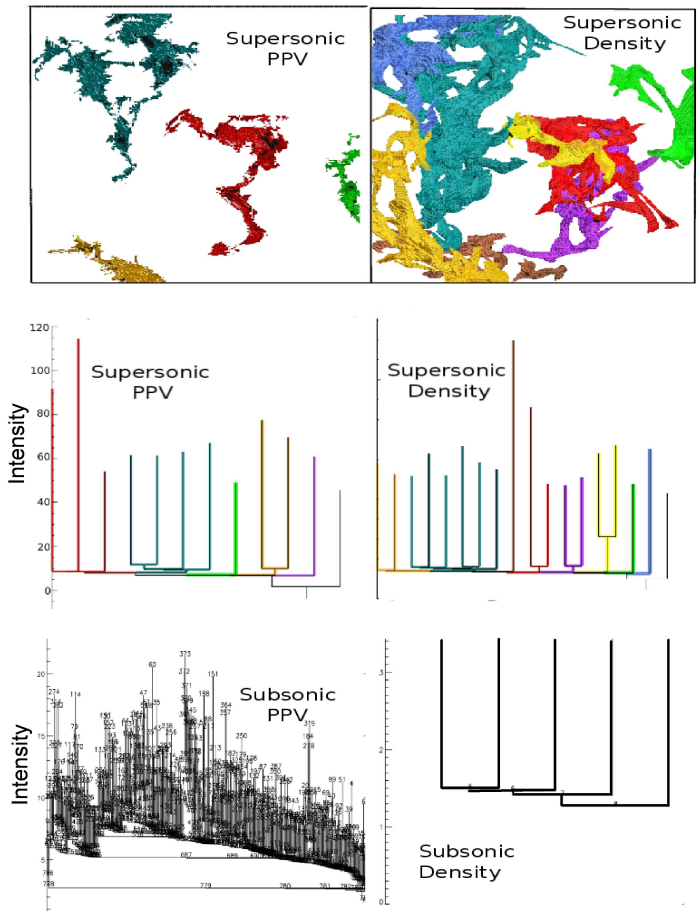

Fig. 11.— Dendrograms of density (right column) and PPV (left column). Supersonic isosurfaces and their corresponding dendrograms are shown in the top and middle rows. Colors are correspondent between structures in the isosurface figures and the dendrogram. Subsonic dendrograms are shown in the bottom row.

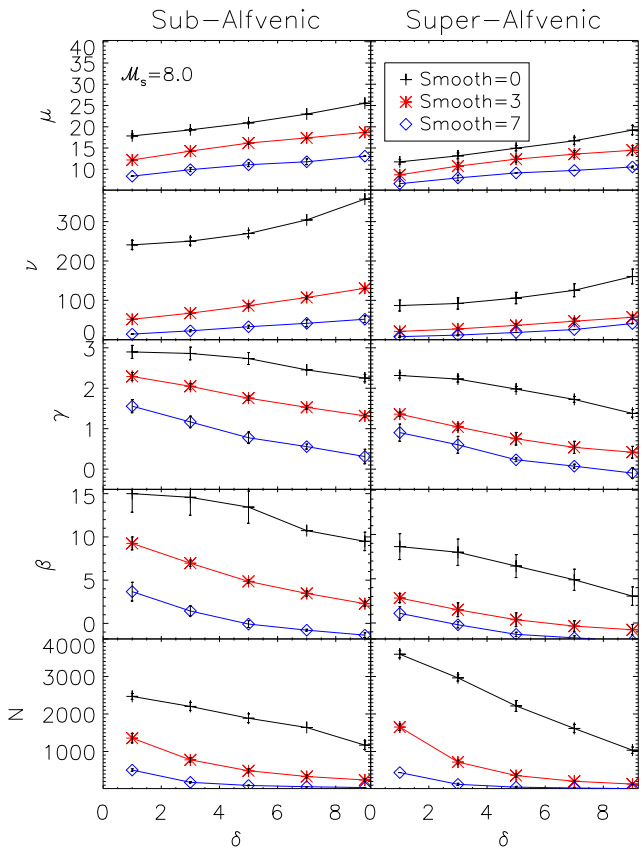

Fig. 12.— Change in the moments dendrogram distribution and the number of structures with smoothing vs. the threshold parameter δ . The left panel is sub-Alfvénic and the right panel is super-Alfvénic and the y-axis is the same for both columns for ease of comparison between the two. Both cases have $\mathcal{M}_s$=8.0.

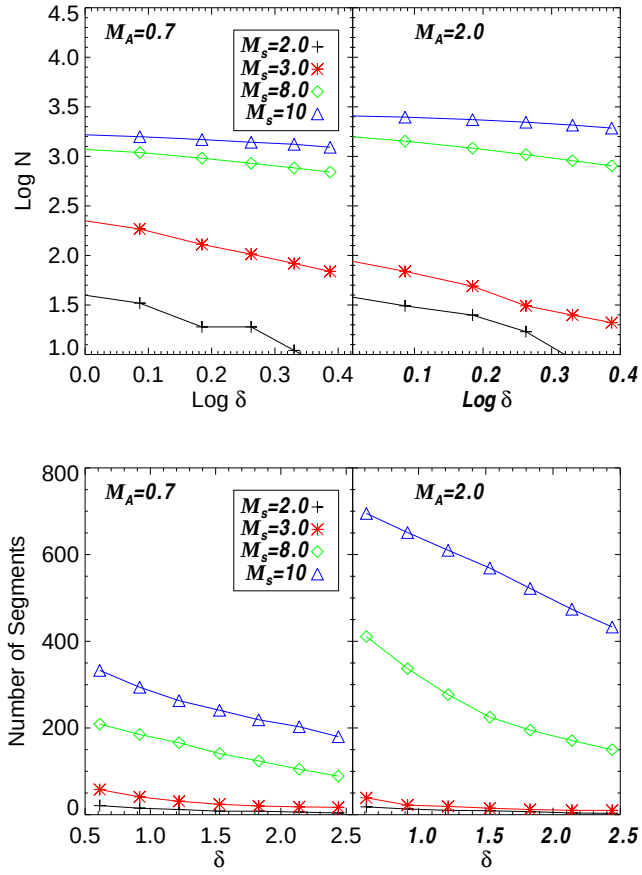

Fig. 13.— Top: Total number of structures (leaves and branches) vs. δ. Bottom: Number of segments from root to leaf on the largest branch of the tree vs. δ. Both plots are similar to Figure 4, only here we include the effects of thermal broadening. In both top and bottom plots the left panel is shows higher magnetization (sub-Alfvénic) while the right shows lower magnetization (super-Alfvénic). Both panels have the y-axis set to the same range for ease of comparison. Hierarchical structure and overall structure is created both by shocks and a high Alfvénic Mach number, even when thermal broadening effects are included.